Ore Geology Reviews 137 (2021) 104288

Contents lists available at ScienceDirect

Ore Geology Reviews

journal homepage: www.elsevier.com/locate/oregeorev

Geological setting and mineralization characteristics of the Tick Hill Gold Deposit, Mount Isa Inlier, Queensland, Australia

Truong X. Le [a,b,*], Paul H.G.M. Dirks [a], Ioan V. Sanislav [a], Jan M. Huizenga [a,c,d], Helen A. Cocker [a], Grace N. Manestar [a]

[a] EGRU (Economic Geology Research Centre), College of Science and Engineering, James Cook University, Townsville, Queensland 4811, Australia
[b] Faculty of Geosciences and Geology Engineering, Hanoi University of Mining and Geology, Hanoi, Viet Nam
[c] Department of Geology, University of Johannesburg, PO Box 524, Auckland Park, 2006 Johannesburg, South Africa
[d] Faculty of Environmental Sciences and Natural Resource Management, Norwegian University of Life Science, P.O. Box 5003, NO-1432 Ås, Norway

ARTICLE INFO

Keywords:
Mt Isa
Mary Kathleen
Tick Hill
Gold deposit

ABSTRACT

The high grade (~22.5 g/t), gold-only Tick Hill deposit presents a unique mineralization style in the Mt Isa Inlier. The deposit was mined in the early 1990s, and is hosted in biotite schist, calc-silicate gneiss, quartzite and quartz-feldspar mylonite. These rocks were affected by D_1 shearing and D_2 upright folding at high-grade metamorphic conditions, followed by D_3 events including normal faulting with widespread quartz-feldspar alteration and D_4 strike-slip faulting. The Tick Hill ore body was linear in shape and paralleled the D_1 mineral elongation lineation, and the intersection lineation between sets of D_3 faults. Gold is dominantly hosted within intensely silicified units affected by D_3 fracturing and associated alteration. However, some gold grains are contained within syn-D_1, peak-metamorphic minerals indicating that mineralization involved two separate events; an early event pre-dating or concomitant with D_1 when gold was first introduced and concentrated, and a second event during D_3 when gold was remobilized and/or further enriched to be deposited in its final configuration. Mineralization at Tick Hill is characterized by coarse grained gold associated with Bi-selenides, minor sulfides, and a general paucity of other metals except for a slight enrichment of Cu in the footwall to the ore zone. Alteration is characterized by early silicification and magnetite alteration that formed during the initial $D_{1\text{-}2}$ events and may have coincided with the first stage of gold enrichment. During syn-D_3 (re-)mobilization of gold, alteration involved the destruction of magnetite, the emplacement of abundant laminar quartz veins, and the deposition of proximal albite, hematite, chlorite, amphibole, epidote overprinted by later K-feldspar, sericite, clay minerals and minor calcite. The ore zone is bounded by a strongly silicified zone and surrounded by a chlorite-epidote shell. The low pressure D_3 gold (re-)mobilization event involved an oxidized, S-under-saturated, acidic, saline aqueous fluid. In terms of alteration characteristics, the Tick Hill deposit shares similarities with IOCG deposits in the area. However, its high-grade gold-only nature, lack of Cu, and the presence of Bi-selenides makes it a unique deposit in the Mt Isa Inlier.

1. Introduction

The Mesoproterozoic (1900–1500 Ma) Mt Isa Inlier is one of Australia's foremost mineral provinces and is famous for its world-class Cu-Pb-Zn-Ag deposits (e.g. Mt Isa mine; Huston et al., 2006), structurally modified and metamorphosed SEDEX (e.g. Dugald River, Cannington; Xu, 1996; Walters and Bailey, 1998) and IOCG deposits (e.g. Ernest Henry; Mark et al., 2006). In addition to these, there are many other large deposit including Mo (e.g. Merlin; Babo et al., 2017), Co (Walford Creek; Aeon Metals Limited, 2017), REE/U (Mary Kathleen; Oliver et al., 1999) and gold-rich IOCG's deposits (e.g. Starra; Duncan et al., 2014).

The Mt Isa Inlier also represents one of the most extensively altered terrains on Earth exemplified by widespread albite-hematite-scapolite-epidote alteration, which was linked to the remobilization of evaporite deposits during various deformational and intrusive events (e.g. Oliver et al., 1994; Oliver, 1995; De Jong and Williams, 1995; Withnall and Hutton, 2013). This alteration is accompanied by widespread brecciation, and the syn- to post-tectonic emplacement of both felsic and mafic

* Corresponding author at: EGRU, James Cook University, Townsville, QLD 4811, Australia.
E-mail address: truong.le@my.jcu.edu.au (T.X. Le).

https://doi.org/10.1016/j.oregeorev.2021.104288
Received 16 November 2020; Received in revised form 31 May 2021; Accepted 6 June 2021
Available online 9 June 2021
0169-1368/© 2021 Elsevier B.V. All rights reserved.

intrusions (e.g. Oliver, 1995; Oliver et al., 2008). The alteration and brecciation are characteristic features of the IOCG deposits in the Mt Isa Inlier (Williams et al., 2005) and are hallmarks for many of the other deposit types as well.

Whilst Cu-Au IOCG deposits are common in the Mt Isa Inlier, especially in the higher grade and more strongly deformed Eastern Fold Belt (Fig. 1), gold grades in such deposits rarely exceed 1–2 g/t, and gold-rich deposits are rare (e.g. Duncan et al., 2011; Denaro et al., 2013). One notable exception to this is the Tick Hill Gold Deposit in the southern part of the Mary Kathleen Domain (MKD; Fig. 1). Although the Tick Hill deposit presents a mineralization style of great interest to exploration companies, little is known about the deposit other than that it is a gold-rich, shear-hosted hydrothermal deposit (Denaro et al., 2013) that has been interpreted as a possible end-member IOCG deposit (e.g. Groves et al., 2010). Tick Hill was discovered in 1989, and was mined over a short period (1991–1994). Apart from several student theses (Tedman-Jones, 1993; Watkins, 1993; Choy, 1994) no detailed studies have been published on the deposit or its style of mineralization.

The Tick Hill deposit is situated in high-grade metamorphic rocks and characterized by the occurrence of free gold with little to no silver and a paucity of sulphides and associated metals (e.g. Cu, Co). As such, Tick Hill is a unique gold-rich deposit in the Mount Isa Inlier, which was highly profitable when mined. This study provides an overview of the geological setting and mineralization style of the Tick Hill deposit based on mapping, core logging and petrography. It aims to present details on the orebody geometry in relation to lithological and structural-metamorphic controls, together with a characterization of the gold mineralization and associated alteration.

1.1. Exploration and mining history of Tick Hill

The Tick Hill Gold Deposit is situated at 21° 38′N–139° 55′E, 110 km south-southeast of Mount Isa in northwest Queensland, Australia (Fig. 1). The deposit was discovered by Mount Isa Mines Ltd (MIM, formerly Xstrata, now part of the Glencore Group) in October 1989 after follow up of a *Bulk Leach Extractable Gold* anomaly in a stream sediment sample. Following resource definition, mining commenced in August 1991 and the first gold was poured in December 1991. Open pit and underground mining was done by Carpentaria Gold Pty Ltd and ceased in April 1995. The deposit produced a total of 511,000 oz of gold from

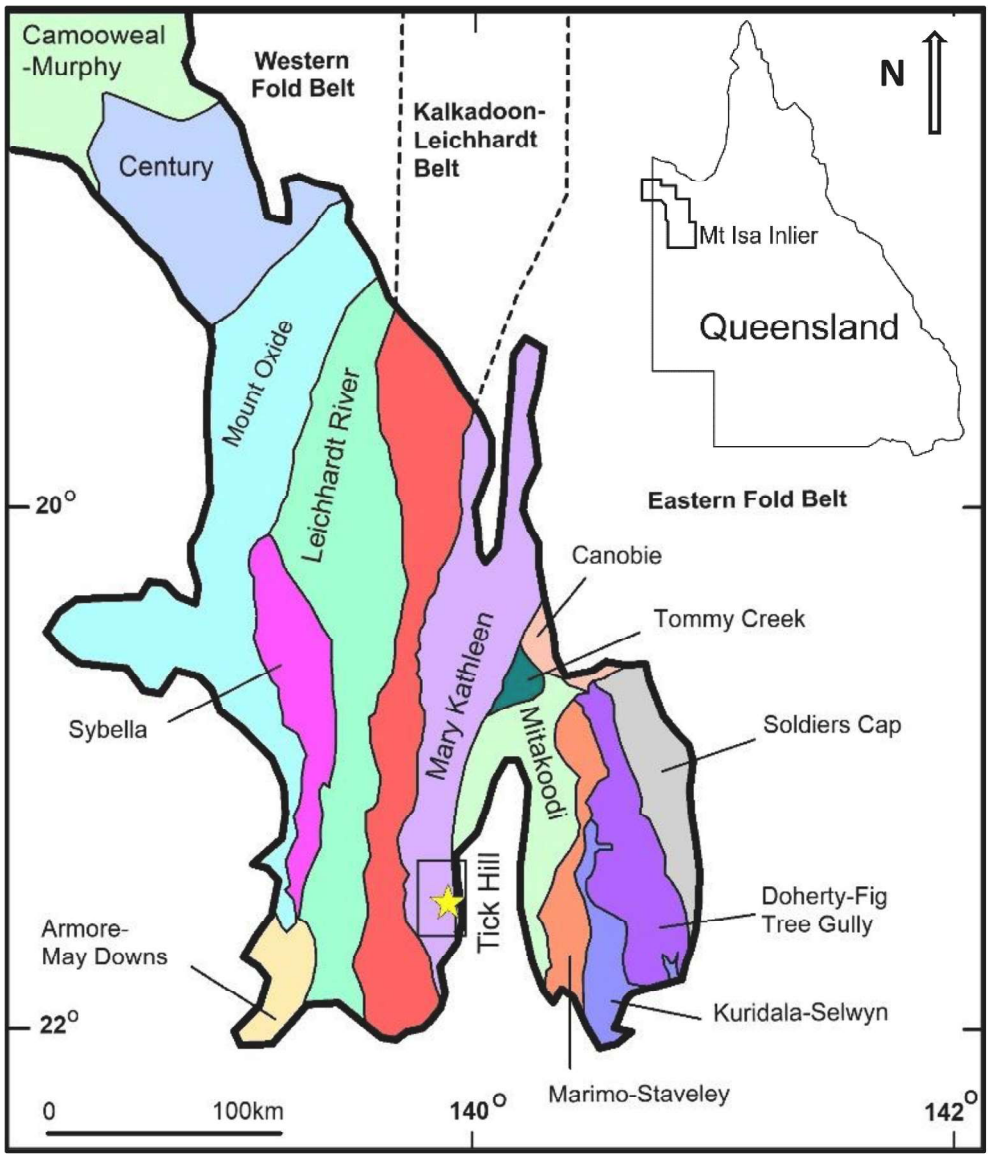


Fig. 1. Tectonic subdivisions of the Mt Isa Inlier as defined by Withnall and Hutton (2013) showing different domains and the boundaries of the Eastern Fold Belt and Western Fold Belt on either side of the Kalkadoon-Leichhardt Belt. The black box shows the area shown in Fig. 2a. The inset map shows the location of the Mt Isa Inlier in relation to Queensland.

706,000 tonnes of ore at an average grade of 22.52 g/t Au. Metallurgical recovery averaged 97% and production costs were low. In 1998–1999 Cullen in joint venture with MIM re-evaluated the deposit and did extensive exploration in the area without any success. In August 2004, Diatreme Resources Limited (DRX) acquired the right to explore for gold in the Tick Hill area. Further drilling around the deposit was unsuccessful, but a limited gold resource was defined in the waste rock piles around the open pit. In March 2019, the mine was obtained by Carnaby Resources, who commenced renewed exploration in the area in June 2019, to declare a remaining resource of 65,000 oz contained in the north wall of the pit and in old tailings (Carnaby Resources, 2021).

Public information on the Tick Hill deposit is limited to several Honours and MSc theses from the early 1990s, several company reports and a few core logs available on-line (e.g. Tedman-Jones, 1993; Watkins, 1993; Choy, 1994; Rutherford, 1999, 2000; Geological Survey of Queensland, 2015). However, there is a significant amount of information contained in mostly confidential exploration reports held by MIM and Carnaby Resources, the principle conclusions of which are reviewed below. The most comprehensive and detailed re-evaluation of the deposit was provided by Tedman-Jones (2001).

The Tick Hill ore body is hosted in fractured and silica-hematite-altered gneiss. The principle host rock to mineralization is a metasomatized quartz-feldspar mylonite that was labelled "galahstone" to denote its laminated pink and grey appearance. It was derived from sheared quartz-feldspar porphyry, pegmatite and/or calc-silicate metasediments (e.g. Laing, 1992; Tedman-Jones, 2001). To emphasise the metasomatic overprint of the mylonite and the presence of thin quartz-feldspar alteration selvedges along the mylonitic fabric, Laing (1992) proposed the term "quartz-feldspar laminite". In a later review of drill core, Tedman-Jones (2001) described the pervasive occurrence of dilation fractures and thin sheeted partings along S_1 mylonite planes, and linked it to the introduction of K-Na feldspar metasomatism and gold.

Tedman-Jones (2001) noted that the high-grade ore zone is associated with the formation of north-northeast- to east-trending fractures, and the ore zone stopped abruptly at the northern end of the open pit where the "galahstone" terminated against an E-trending structure. The mineralization also pinches out at depth as the main foliation, which dips 55° to the west in the upper drives, switches to a northerly dip observed on the two lowest mine levels (130 and 117 mRL). On these levels, coarse-grained gold was mined from fault hosted chlorite-hematite-carbonate breccia veins that formed the keel of the ore zone, and the breccia veins were interpreted as possibly feeder structures (Tedman-Jones, 2001). Laing (1992) and Tedman-Jones (2001) further noted that east (085°)-trending zones of more extensive dilation appear to occur at 10 m intervals across the deposit, and that these fractures are characterized by pervasive pink and red feldspar fill and associated alteration.

Following the discovery of the Tick Hill deposit in 1989, extensive exploration led by MIM failed to locate an economic resource beyond the original discovery. Most exploration for Tick Hill-style mineralization was premised on the assumption that gold mineralization related to early, ductile (D_1 or D_2) deformation events (Tedman-Jones, 2001). Because gold was described as being associated with the peak metamorphic assemblage (e.g. Choy, 1994; Oliver, 1998), it was suggested that the main stage of mineralization was early (interpreted as 1750–1740 Ma), and possibly followed by later remobilization (e.g. England, 1993, 1995; Choy, 1994; Oliver, 1995). In developing an exploration strategy, it was proposed that gold mineralization was deposited from saline oxidized fluids into a dilatant brittle-ductile ramp structure within a flat lying extensional decollement of D_1 origin (e.g. Oliver, 1998). In the Tick Hill area, it was assumed that the hanging wall and footwall quartzite units were the metasomatic expressions of the decollement, and thus the controlling structures (Tedman-Jones, 2001). This approach did not lead to further gold discoveries.

The possibility that gold mineralization was related to later deformation events (D_3 or D_4) was also suggested (e.g. Laing, 1992; Tedman-Jones, 2001). In 1998–1999, Cullen in joint venture with MIM investigated late stage mineralization concepts, and focused on a possible association between gold, porphyry systems and red rock alteration associated with brittle structures (Tedman-Jones, 2001), but again this work did not lead to further discoveries.

The MIM exploration efforts were reviewed by Tedman-Jones (2001) and Johnson (2002) who concluded that gold mineralization was introduced by late, relatively low temperature, oxidized hydrothermal brines. Tedman-Jones (2001) linked the mineralizing fluids to a granite intrusion at depth, immediately southwest of the Tick Hill deposit. Evidence for an intrusive source comes from geophysical interpretations (Nano, 1999) supported by oxygen isotope studies (Hannan, 1994). Aeromagnetic data obtained by MIM in the late 1990s showed that the Tick Hill orebody is located at the northeastern margin of a 3 × 2 km oval shaped zone of magnetic depletion interpreted to be the expression of a concealed intrusion (Nano, 1999). Hannan (1994) reported a narrow range of $\delta^{18}O_{VSMOW}$ values (+10.2 to +12.9‰) for quartz separates from Tick Hill mine (ore zone and altered surrounding rocks) and suggested that gold formed from a single fluid over a narrow temperature range close to 450 °C. A similar range of quartz $\delta^{18}O$ values from the ore zone was reported by Choy (1994), who proposed a granitic source for the fluids.

2. Geological setting

2.1. Regional geological setting

The Mount Isa Inlier in northwest Queensland exposes complexly deformed, strongly altered and extensively mineralized, mid-Proterozoic rocks that comprise at least three separate basinal sequences (originally referred to as Cover Sequences 1–3; Blake, 1987) deformed by two orogenic cycles (Etheridge et al., 1987; Foster and Austin, 2008). The inlier was originally sub-divided into three, north-trending tectonic units including the Western Fold Belt, the central Kalkadoon-Leichhardt Belt and the Eastern Fold Belt (Day et al., 1983), to delineate large-scale subdivisions with broadly similar tectono-stratigraphic histories. These subdivisions were further split into a series of geological domains based on stratigraphic, structural and geochronological similarities (Fig. 1; Withnall and Hutton, 2013). Thus, the Eastern Fold Belt, which occurs east of the Kalkadoon-Leichardt Domain, comprises eight domains including the Mary Kathleen Domain (MKD) that hosts the Tick Hill deposit (Fig. 1). To the west, the metasedimentary rocks of the MKD uncomfortably overlie rocks of the Kalkadoon-Leichhardt Domain (Withnall and Hutton, 2013). To the east, the MKD is separated from the rest of the Eastern Fold Belt by the Pilgrim Fault in the south and the Rose Bee Fault in the north (Withnall and Hutton, 2013).

The Tick Hill deposit is situated in the southern part of the MKD. This part of the MKD is relatively poorly studied and stratigraphic and tectonic interpretations for rocks around Tick Hill largely rely on lateral correlations with better studied rocks further north (e.g. Passchier, 1986, 1992; Passchier and Williams, 1989; Holcombe et al., 1991; Neumann et al., 2009; Carson et al., 2011; Withnall and Hutton, 2013; Kositcin et al., 2019). In the central part of the MKD, gneiss of the Kalkadoon-Leichhardt complex, and overlying mafic and felsic volcanics of the Magna Lynn metabasalt unit, and the 1770–1780 Ma Argylla Formation (e.g. Page, 1978; Neumann et al., 2009), form basement to unconformably overlying shallow water sediments (e.g. Withnall and Hutton, 2013). These consist of the ca. 1755 Ma Ballara Quartzite and extensive deposits of the 1738–1750 Ma Corella Formation (Blake et al., 1982; Foster and Austin, 2008; Neumann et al., 2009; Withnall and Hutton, 2013; Kositcin et al., 2019). In the central MKD, the Corella Formation is composed of scapolitic-bearing calc-silicate, para-amphibolite, marble, metapelite, quartzite and other metasedimentary units with minor felsic and mafic metavolcanics (Blake, 1987; Foster and Austin, 2008). The correlative stratigraphic unit of the Corella

Formation in the area around Tick Hill has not been dated directly and its age has been interpreted (e.g. Wyborn, 1997; Foster and Austin, 2008). Intrusions in the southern MKD have been grouped into granites assigned to the ca. 1740 Ma Burstall-Wonga Suite (e.g. Monument Syenite, Saint Mungo Granite, Birds Well Granite and Tick Hill Granite; Fig. 2) and Kalkadoon Batholith, which mostly occurs to the west of Tick Hill (e.g. Blake et al., 1982; Wyborn, 1997; Withnall and Hutton, 2013).

The metamorphic and deformational history of the MKD involved four major deformational events (D_1 to D_4; e.g. Passchier and Williams, 1989; Holcombe et al., 1991; Oliver, 1995). The early D_1 event (interpreted as 1750–1730 Ma) has been interpreted as extensional in nature, and has been linked to an early gneissic fabric exposed in high strain zones along the central part of the MKD termed the Wonga-Shinfield zone (Passchier and Williams, 1989; Holcombe et al., 1991). Upright folding occurred during D_2 and was originally interpreted to relate to the main stage of the Isan Orogeny around 1590–1550 Ma, when peak

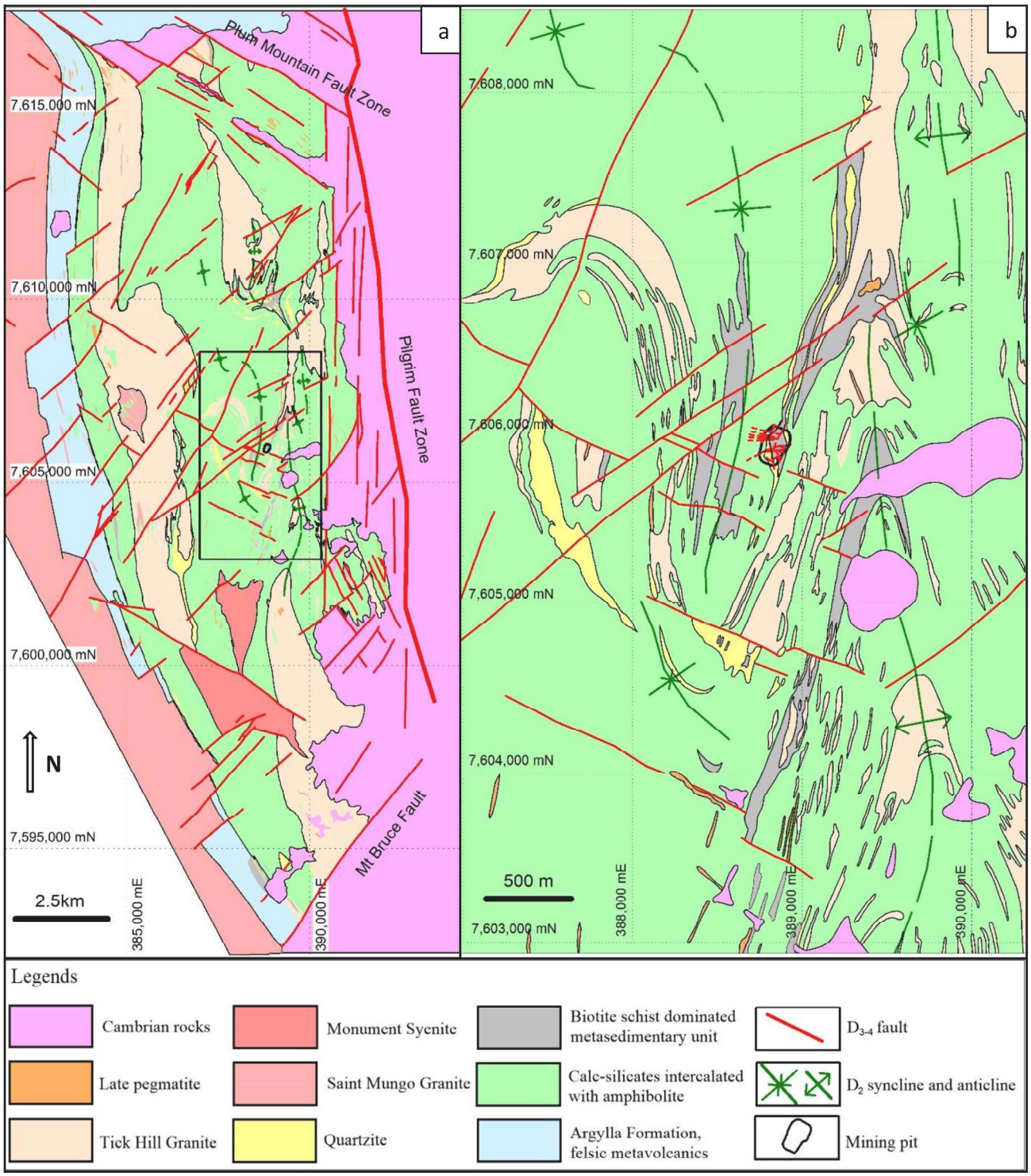


Fig. 2. (a) Geological map of the Tick Hill area with (b) a close-up of the Tick Hill Syncline area. Note that the calc-silicate, amphibolite, biotite schist and quartzite units were interpreted as the Corella Formation while the felsic metavolcanics were assigned to the Argylla Formation (adapted from Wyborn, 1997; Rutherford, 2000).

metamorphic conditions were attained (e.g. Page, 1983; Passchier and Williams, 1989; Holcombe et al., 1991; Oliver, 1995). More recently, however, Pence et al. (2020) have shown that D_2 upright folding in the central MKD took place before 1710 Ma. The D_2 deformation resulted in the development of upright, tight, north-trending folds with an axial planar cleavage, a penetrative S_2 fabric, and steep east-dipping reverse faults parallel to F_2 fold axial planes (e.g. Holcombe et al., 1991; MacCready et al., 1998). D_3 events marked a change from ductile to brittle deformation and led to the formation of a fault network (O'Dea et al., 1997; Betts et al., 2006). In the southern MKD, the Wonga-Shinfield zone was offset by a series of northeast and northwest striking D_3 faults in response to east–west compression (Forrestal et al., 1998). D_3 events were coeval with the regional emplacement of the Wimberu/Williams granite plutons (1530–1500 Ma; Foster and Austin, 2008) to the east and related regional albite-hematite-alteration (Wyborn et al., 1988). D_4 events involved brittle reactivation of older fault zones at shallow crustal levels, at temperatures <350–400 °C, with the suggested age of deformation ranging from 1500 Ma to 1100 Ma (e.g. Oliver, 1995).

2.2. Geological setting of the Tick Hill area

The Tick Hill area is underlain by rocks interpreted as Corella Formation bounded in the east by the Pilgrim Fault and in the west by granitic gneiss of the Saint Mungo Granite overlain by felsic volcanics assigned to the Argylla Formation (Coughlin, 1993; Wyborn, 1997). To the north, the area is bounded by the northwest-trending Plum Mountain Fault and to the south by the northeast-trending Mt Bruce Fault (Fig. 2a; Forrestal et al., 1998). The rocks of the Corella Formation were intruded by syn-tectonic (i.e. syn-$D_{1\text{-}2}$) Tick Hill Granite and Monument Syenite and post-tectonic pegmatite (Fig. 2a; Wyborn, 1997; Rutherford, 2000). Cambrian rocks outcrop to the east of the Pilgrim Fault and are locally preserved as erosion remnants overlying the Corella Formation to the east of the Tick Hill pit (Fig. 2a).

Detailed mapping of the Tick Hill area and the surrounding geology during exploration by MIM (Fig. 2; Coughlin, 1993; Rutherford, 2000) led to the development of a D_1 to D_4 deformation sequence that was linked to the regional tectonic framework further north. Around Tick Hill, D_1 refers to the development of the mylonitic gneissic fabric, which is prominently developed in the rocks that host the Tick Hill deposit. The mylonite formed along a north-trending belt, west of the Pilgrim Fault, and is characterized by a prominent S_1 foliation with a westerly dip (around 280/60; all orientation measurements for planes are presented as dip direction/dip) and a well-developed steeply southwest pitching mineral lineation and/or rodding lineation (L_{1x}). The fabric is defined by oriented hornblende-plagioclase-clinopyroxene assemblages in meta-basalt, and silimanite-biotite-scapolite in meta-sediments. Numerous quartzo-feldspathic horizons and sheared leucogranite layers suggest the presence of abundant granite melt pockets, that either formed as the result of local migmatisation, granite intrusions or both (Fig. 2). Intrafolial folds and sheath folds in the mylonitic fabric can be observed on centimeter to meter scale, and in places several overprinting generations of intrafolial folds have been described (e.g. Choy, 1994; Oliver, 1998). F_1 fold axes associated with the intrafolial folds are commonly parallel to the mineral lineation. The D_1 high strain fabric has been linked to the Shinfield-Wonga belt north of Tick Hill, and it was interpreted as an expression of the ca. 1740 Ma, mid-crustal extensional shear zone (e.g. Oliver, 1998). The D_1 mylonites were folded during D_2 in a series of km-scale, tight, asymmetric upright folds. The Tick Hill deposit is situated in the eastern limb of one such large D_2 syncline (the Tick Hill syncline; Fig. 2b), which has an axial planar trace that parallels the D_1 gneissic fabric (Choy, 1994). The D_2 folds tighten and intensify west of the Tick Hill pit, where they become transposed in a north-trending high strain zone that parallels the S_1 fabric, suggesting that D_1 and D_2 events may be expressions of a single, progressive shearing event (Laing, 1993). D_2 folds open up towards the Pilgrim Fault to the east. Later deformation events (D_3 and D_4) were described as northwest- and northeast-trending fault sets with associated red rock alteration (Tedman-Jones, 2001). The main D_3 structures bound the Tick Hill area to the north and south (Fig. 2). Within the deposit, D_3 is manifested as an interconnected network of fractures and veins with associated quartz-feldspar alteration and gold mineralization (Tedman-Jones, 2001). D_4 deformation includes a series of strike-slip faults that trend northeast, and offset the D_1 Tick Hill gneiss fabric and D_2 fold axes (Coughlin, 1993), and overprinted the D_3 red rock alteration (Tedman-Jones, 2001).

3. Geological framework for the Tick Hill deposit

The deformation scheme and lithological descriptions presented here are based on mapping of the Tick Hill pit in November 2017, together with drill core logging of a limited number of available cores, and petrological studies. This is augmented with regional maps compiled by MIM in the 1990s (Fig. 2; Coughlin, 1993; Rutherford, 2000).

3.1. Lithological units in Tick Hill pit

The host rocks to the Tick Hill deposit as exposed in the pit and its immediate surroundings, consist of gneissic and schistose units that have been interpreted as part of the Corella Formation (e.g. Coughlin, 1993; Choy, 1994; Wyborn, 1997; Figs. 2 and 3). They include from west to east (i.e. from hanging wall to footwall): (1) a hanging wall calc-silicate unit interlayered with amphibolite gneiss, (2) hanging wall quartzite, (3) a central metasedimentary unit dominated by biotite schist, (4) footwall quartzite, and (5) footwall calc-silicate interlayered with amphibolite gneiss. The ore zone is largely contained within the central biotite schist unit, where it is interlayered with quartz-feldspar mylonite that is similar in composition as the nearby Tick Hill Granite Complex (Le et al., 2021) and probably of intrusive origin. The origin of the quartzite ridges is uncertain, and most exploration reports refer to them as metasomatic alteration zones, rather than sedimentary units, citing their cross-cutting, discontinuous nature (e.g. Laing, 1993; Coughlin, 1993; Oliver, 1998). All units are truncated by weakly deformed quartz and pegmatite veins. The distribution of the various lithologies in the pit is presented in Fig. 3 and the peak-metamorphic mineral assemblages in each rock unit are listed in Table 1.

3.1.1. Hanging wall calc-silicate interlayered with amphibolite gneiss

This unit is well-exposed in the west wall of the pit, and in many drill cores. The unit comprises banded or laminated gneissic calc-silicate and amphibolite, interbedded with lesser biotite schist, and can be subdivided into amphibolite, amphibole-rich calc-silicate, calc-silicate, and magnetite-rich calc-silicate sub-units (Fig. 4).

The gneissic amphibolite sub-unit is best exposed along the top benches of the open pit where it overlies calc-silicate (Fig. 3a). The amphibolite is strongly foliated, with the foliation defined by oriented hornblende, which comprises 50–80% of the rock (Figs. 4a, 5a). Other minerals include plagioclase, scapolite, quartz, magnetite, actinolite, garnet and accessory minerals including zircon and apatite (enclosed in quartz). Locally, the amphibolite sub-unit displays variations in composition on m-scales, with quartz-rich (>10% quartz) amphibolite horizons alternating with plagioclase-rich or calc-silicate-rich horizons.

The gneissic calc-silicate sub-unit (Fig. 4b) constitutes the bulk of the rock in the sequence above the hanging wall quartzite, and is well-exposed in the west wall of the pit (Fig. 3a). The general composition of the calc-silicate is feldspar (40–60%), scapolite (20–35%), quartz (10–15%), magnetite (<3–4%) and variable amounts of hornblende, actinolite and chlorite (Fig. 5b). The scapolite content is highly variable from one layer to the next. Where scapolite is most abundant it preserves a spotty texture, with individual grains aligned within the foliation. Hornblende occurs in discontinuous patches along the gneissic foliation and locally defines the mineral lineation (Fig. 4b). Amphibole-rich layers consisting of quartz-feldspar-amphibole (±scapolite, biotite, and

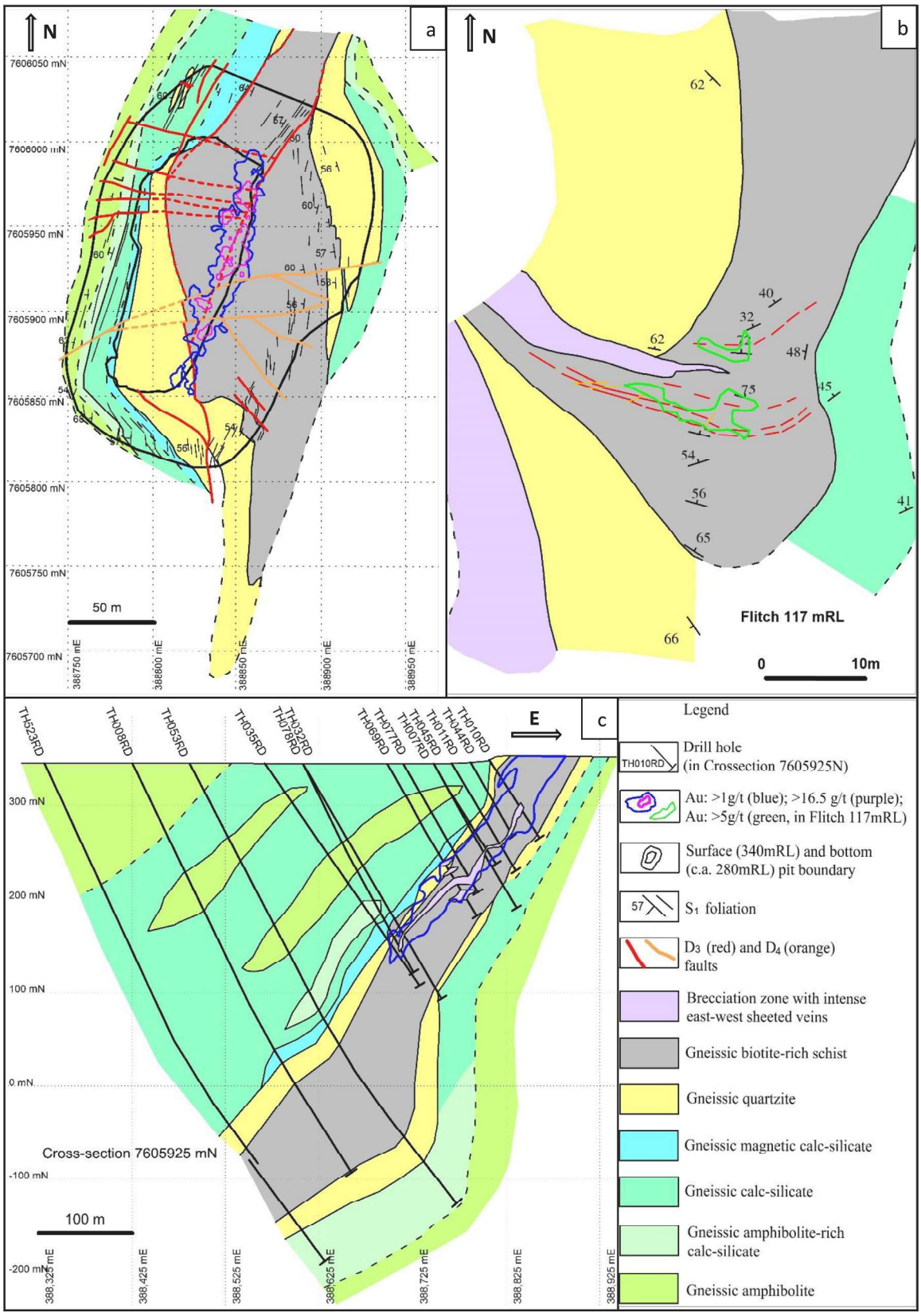


Fig. 3. Geology of the Tick Hill deposit: (a) Geological map of Tick Hill Pit as exposed in November 2017. The surface elevation corresponds to mine level 340 mRL; (b) Underground geological map of level 117 mRL towards the base of the mine, showing a shift of the ore zone from a north-northeast trend at surface to an east-trend that coincides with the D_3 faults (adapted from MIM, 1993); (c) Cross-section 7,605,925 mN showing the lithological host rocks in spatial relationship with the 1 g/t ore envelope and brecciation zones. Drill holes are projected onto the section from 20 m north and south (adapted from Downs, 2000). The 1 g/t ore envelope is hosted in biotite schist and hanging wall quartzite. D_3 brecciation zones and east-trending, sheeted veins coincide with the ore zone.

Table 1
Peak-metamorphic and early (syn-$D_{1\text{-}2}$) alteration mineral assemblages in major rock units. Qtz-fsp = quartz-feldspar.

Minerals	*$D_{1\text{-}2}$ Biotite schist*	*$D_{1\text{-}2}$ Calc-silicate*	*$D_{1\text{-}2}$ Amphibolite*	*$D_{1\text{-}2}$ Qtz-fsp mylonite*
Sillimanite				
Biotite				
Amphibole				
Plagioclase				
K-feldspar				
Quartz				
Diopside				
Scapolite				
Garnet (Almandine > Pyrope > Grossular)				
Apatite				
Magnetite				
Ilmenite (±Mn)				
Gold (inclusion)				
Chalcopyrite				
Pyrite				

Quantity: Dominant — *Minor*

magnetite) occur as intervals in the more massive calc-silicate sequence. The calc-silicate sub-unit is generally altered and overprinted by sericite and clay after feldspar, and chlorite-hematite-goethite after amphibole-biotite-magnetite. The calc-silicate is locally intercalated with layers of biotite-schist, but they are too thin and laterally too discontinuous to be mapped as separate units.

The magnetite-rich calc-silicate sub-unit occurs directly above the hanging wall quartzite unit and locally reaches a thickness of 30 m. This sub-unit is similar in composition to calc-silicate except that the magnetite content is much higher. In drill core (e.g. Geological Survey of Queensland, 2015), the magnetite concentration increases toward the contact with the hanging wall quartzite, to form a 4–6 m wide contact zone consisting of discontinuous, semi-massive to massive granular magnetite lenses (Figs. 4c, 5c). The magnetite-rich calc-silicate is locally intercalated with thin bands of magnetite-bearing amphibolite. Magnetite is aligned in the gneissic fabric and appears to have formed as an early alteration product overprinting and replacing the dominant rock forming minerals, as shown by the presence of abundant inclusions of magnetite in biotite.

3.1.2. Hanging wall quartzite

The hanging wall quartzite unit is best exposed in the south wall of the pit, and in drill cores. The hanging wall quartzite has been intensely deformed and in the immediate hanging wall to mineralization it has been affected by quartz-feldspar alteration. The unit is grey-white in colour and dominated by quartz, but it varies in the composition of secondary minerals that occur as inclusions in quartz. Thus, the quartzite is locally enriched in biotite, or hornblende-chlorite-epidote or feldspar, with inclusion phases aligned in the gneissic layering and partly overgrown by quartz (Fig. 4d). The quartzite is magnetite-bearing along the contact with the overlying calc-silicate unit, but the magnetite content of the rock decreases away from the contact, to form a weakly magnetic middle interval of glassy quartzite. This middle interval is discontinuous along strike, and the magnetite-rich quartzite locally occurs directly above the mineralized zone, especially in amphibolite-rich areas. Intercalations of silicified biotite schist are locally common. The hanging wall quartzite displays an annealed granoblastic texture, in which the dominant foliation is only weakly preserved. It can be intensely brecciated and pervasively altered resulting in a spotty texture. The effects of this alteration are well exposed in the upper benches in the southeast corner of the pit (Fig. 3a). Where alteration is prevalent, chlorite and hematite appears, and feldspar has been altered to sericite and clay minerals.

3.1.3. Biotite schist

The biotite schist unit is well exposed in the north wall of the pit, and is a major host rock to mineralization. However, the strongly altered and mineralized varieties of this unit (including the high-grade ore zones or “galahstone”) can only be seen in drill cores. The biotite schist unit is located between the hanging wall and footwall quartzite units (Fig. 3a), and comprises three sub-units: (1) quartz-feldspar-biotite-amphibole schist (i.e. meta-psammite); (2) biotite-schist that locally contains sillimanite (i.e. meta-pelite); and (3) quartz-feldspar mylonite, which is probably of intrusive origin and commonly gold-rich (Le et al., 2021). Other minor intercalations include amphibolite gneiss and quartzite.

The quartz-feldspar-biotite-amphibole schist sub-unit occurs along the base of the hanging wall quartzite, between the quartzite and the ore zone. The transition from the hanging wall quartzite to biotite schist is gradational and the exact contact is masked by silicification. The least altered parts of this sub-unit contain a fine-grained, light-tan, massive to weakly foliated arkose siltstone or arenite (Fig. 4e). The composition varies laterally and includes quartz (35–60%, including secondary quartz due to silicification), feldspar (15–20%), biotite (5–20%), amphibole (10–20%) and magnetite (±ilmenite, 2–3%). Oriented biotite, amphibole and quartz define a strong schistose fabric.

Biotite schist commonly occurs below the quartz-feldspar-biotite-

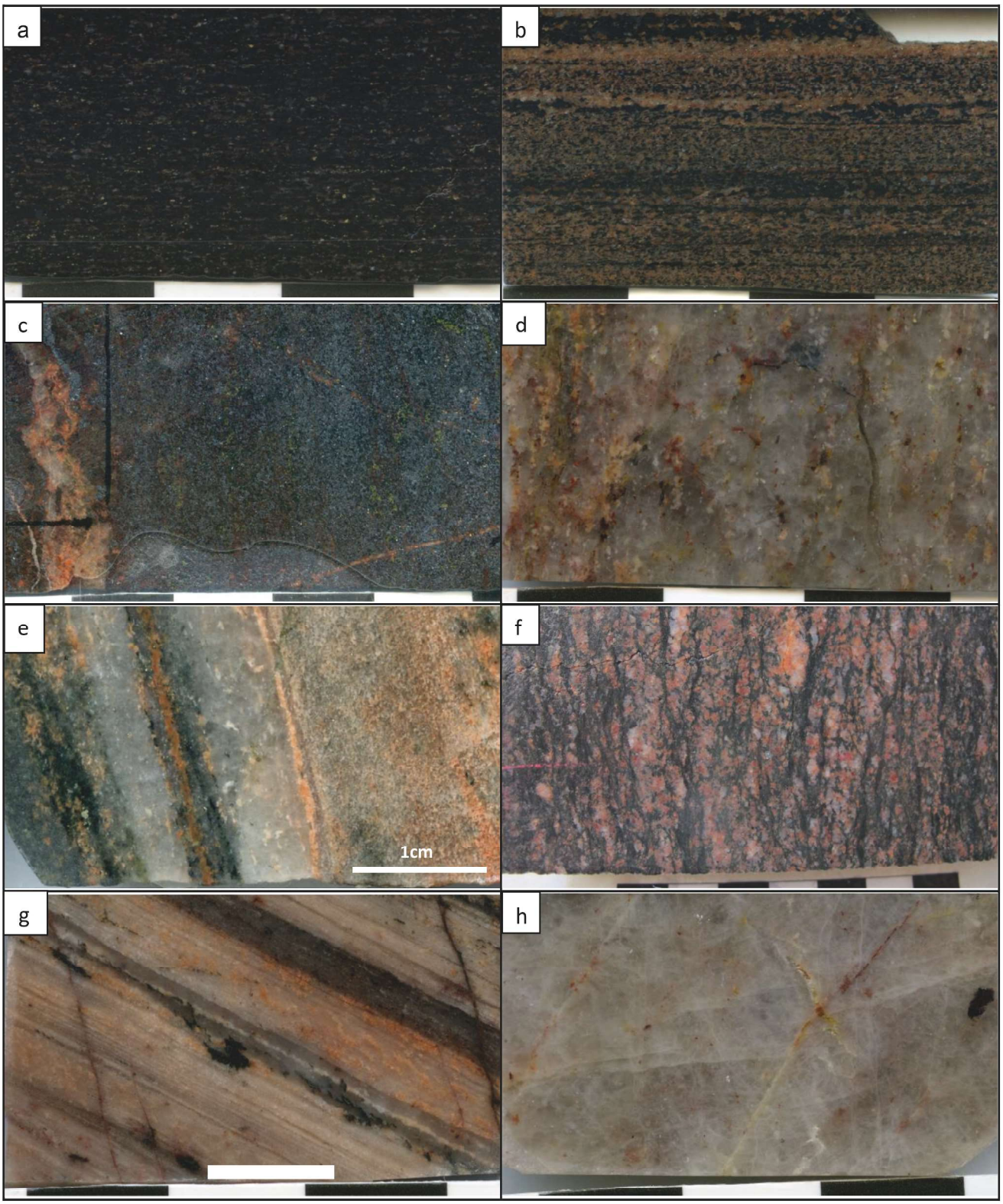


Fig. 4. Rock units from Tick Hill: (a) Gneissic amphibolite with amphibole and plagioclase defining S_1; (b) Gneissic calc-silicate with amphibole, scapolite, plagioclase defining S_1; (c) Amphibole-rich calc-silicate consisting of amphibole-rich bands interlayered with calc-silicate bands that consist of amphibole-quartz-plagioclase-scapolite-magnetite; (d) Hanging wall quartzite showing distributed feldspar grains affected by quartz replacement; (e) Quartz-feldspar-biotite-amphibole schist sub-unit within the biotite schist; (f) Biotite schist in the pit wall composed by biotite, feldspar, sillimanite and amphibole, overprinted by red-rock alteration; (g) Quartz-feldspar mylonite, with feldspar-quartz laminae intercalated with thin quartz vein that have the appearance of ribbon grains. (h) Foot wall quartzite composed of strongly recrystallized granoblastic quartz.

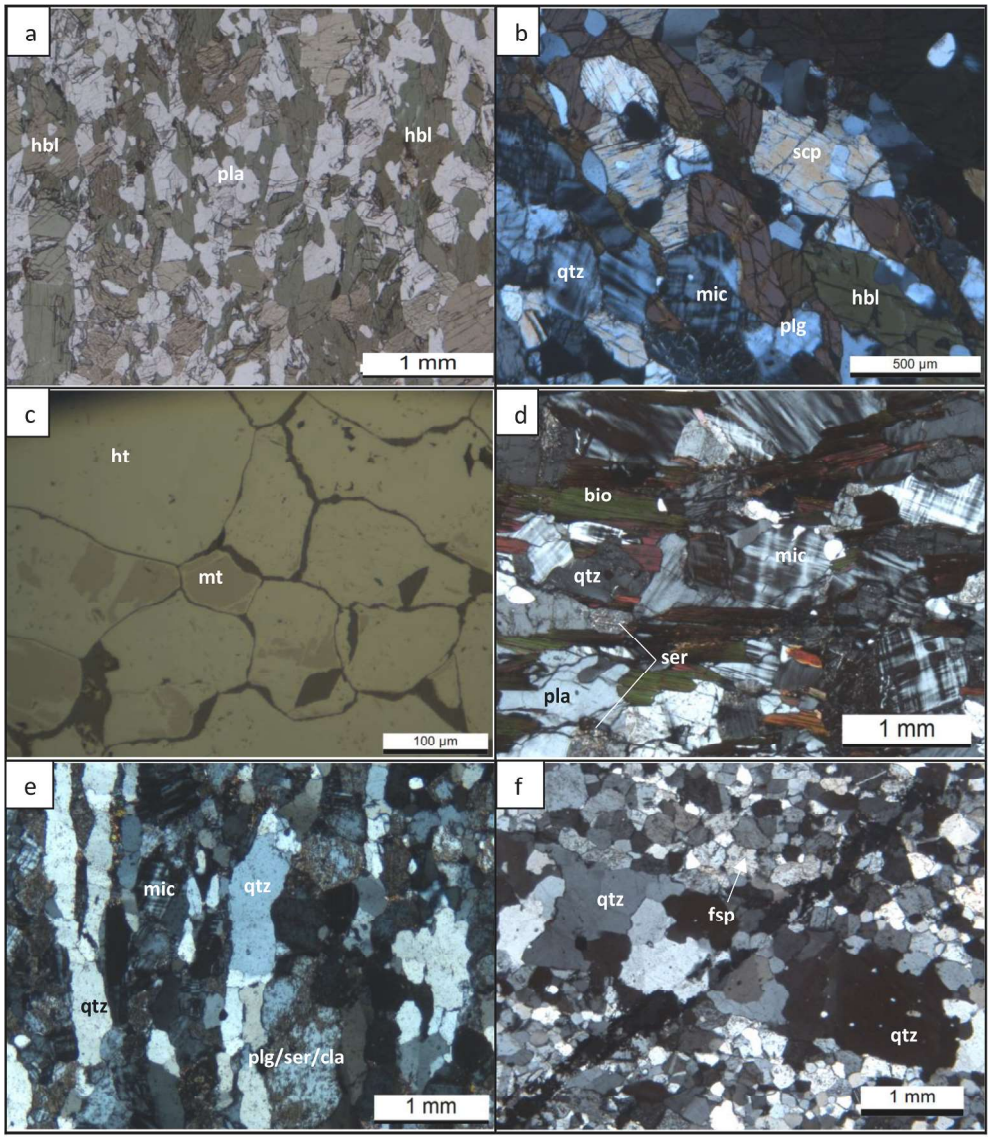


Fig. 5. Photos of thin sections for rock units from Tick Hill: (a) Foliated (S_1) amphibolite composed of hornblende (hbl) and plagioclase (pla); (b) Foliated (S_1) amphibole-rich calc-silicate with scapolite (scp), hornblende (hbl), plagioclase (pla), microcline (mic) and quartz (qtz); (c) Magnetite (mt) in the magnetic calc-silicate sub-unit was replaced by hematite (ht); (d) Foliated (S_1) biotite schist composed of quartz (qtz), biotite (bio), microcline (mic) and plagioclase (pla). The fabric displays annealing textures in which quartz-feldspar grain growth was restricted by biotite grains. Feldspar is partially altered to sericite (ser); (e) Quartz-feldspar mylonite composed of ribbon grains of quartz (qtz), microcline (mic) and plagioclase (pla) that was altered to sericite and clay minerals (cla); (f) Quartz-feldspar mylonite cut by a thin quartz vein (running left to right) that parallels the main mylonitic fabric, and a later fracture filled with opaques (bottom left to upper-right). The quartz displays a granoblastic textures reflecting post-deformational annealing and recovery.

amphibole schist, close to or coinciding with the high-grade ore zone, and it extends into the footwall of the ore zone. Biotite-rich varieties occur along layers, and sillimanite is locally abundant, especially in footwall zones to the ore body (Fig. 4f), although much of the sillimanite has been replaced by muscovite. Within the ore zone, the biotite schist has been intensely silicified and chlorite-hematite altered and the older mylonitic texture has been strongly recrystallized into an interlocking texture of granoblastic quartz grains. The biotite sub-unit generally consists of fine- to coarse-grained biotite and/or biotite-amphibole (30–80%), with quartz (<30%) and feldspar (K-feldspar and plagioclase, <50%) that was partially altered to sericite and clay minerals (Fig. 5d).

The quartz-feldspar mylonite sub-unit is the principle host to gold mineralization in the sequence and occurs as layers within biotite schist. It consists of equal amounts of quartz and feldspar (albite and oligoclase) that occur as discontinuous ribbon grains interlaminated with thin quartz bands (Figs. 4g, 5e). Individual quartz and feldspar lamellae generally do not exceed 3 mm in width, and they are mostly thinner than that, but in places quartz-rich or feldspar-rich bands (or veins) can be up to 10 cm thick. Feldspar consists of albite with minor K-feldspar and Na-rich oligoclase. The quartz-feldspar mylonite is characterized by a sugary, granoblastic texture reflecting post-deformational annealing and recovery (Fig. 5f). In places, the recrystallized fine-grained quartz-feldspar mylonite is truncated by, or overprinted by laminated thin (<2 mm) partings of grey quartz, which formed parallel or at low angles to the original mylonitic foliation (i.e. the "laminate" of Laing, 1992). The composition of the quartz-feldspar mylonite suggests that it originated as intrusive granite sheets or granitic migmatite (Le et al., 2021).

3.1.4. *Footwall quartzite*

This unit is best exposed in the northeast corner of the pit. Most drill cores do not penetrate this unit, limiting descriptions to field observations. The thickness of the footwall quartzite varies along strike and with depth and it pinches out towards the southern end of the pit (Fig. 3a). The unit is thickly bedded (>30 cm), and consists of grey-white translucent orthoquartzite (Fig. 4h) with traces of biotite, magnetite and heavy minerals including zircon and apatite. The unit has a granoblastic texture with a common grain size of 150–350 μm, and has been strongly deformed, but it lacks the spotty texture resulting from abundant inclusions of feldspar, magnetite, hornblende or biotite, and alteration, which characterizes the hanging wall quartzite.

3.1.5. *Footwall calc-silicate interlayered with amphibolite gneiss*

This unit is not exposed in the pit, and few drill cores penetrate it. The unit is similar in appearance to the various calc-silicate and amphibolite lithologies described above. In the immediate footwall to

the footwall quartzite unit, calc-silicate lithologies dominate, whilst away from the quartzite the unit is transitional into amphibolite (Fig. 3a).

3.1.6. Late pegmatite veins

The gneiss units in the Tick Hill pit were intruded by late-tectonic pegmatite dykes, and the gneissic layering is locally overprinted by pegmatite-like metasomatic alteration zones, which developed as rims along late fractures. Although somewhat deformed and locally boudinaged, the pegmatite veins exhibit no penetrative, mylonitic deformation fabrics and they transect the pervasive gneissic layering that characterizes the host rocks.

Late pegmatite veins occur as thin (<0.6 m) dyke-like bodies and preserve a fine- to medium-grained texture of intergrown feldspar-plagioclase and quartz near the margins of the dykes with a core dominated by plagioclase (85–95%) with variable amounts of quartz (<10%), K-feldspar (<5%) and biotite (0–10%). In drill core, pegmatite-like veins appear in the footwall of the ore body and are associated with metasomatized zones with a granular texture and diffuse boundaries in which feldspar (30–40%), quartz (20–30%) and minor biotite (<5%), overprint and replace the underlying metamorphic fabrics. The late-tectonic pegmatite intrusions were strongly affected by later hydrothermal alteration, in which feldspar was replaced by an albite-sericite assemblage.

3.2. Deformation sequence in the Tick Hill Deposit

Rocks hosting the Tick Hill deposit were affected by four distinct deformation and metamorphic events: (1) D_1 shearing at upper amphibolite to granulite facies metamorphic conditions; (2) D_2 upright folding at upper amphibolite facies metamorphic conditions; (3) D_3 normal faulting with extensional veining and widespread quartz-feldspar alteration at lower amphibolite to upper greenschist facies; and (4) D_4 strike-slip faulting with cataclasite formation along fault planes. Each of the events as seen in the pit and its immediate surroundings, and in drill cores has been described in more detail below.

3.2.1. D_1 events

The dominant structural element in Tick Hill pit and its immediate surroundings is a well-developed, moderately west-dipping schistose or gneissic layering and associated mineral lineation, which formed during the earliest stages of deformation referred to as D_1. This layering consists of an annealed mylonitic fabric with sugary, granoblastic characteristics in quartz-feldspar-rich lithologies (i.e. blasto-mylonites), and has an orientation within the pit that varies from 305/65 (dip direction/dip) to 250/50 (Fig. 6a). The layering is a composite tectonic fabric and locally contains isoclinal intrafolial folds, which are best preserved within the calc-silicate unit. Around the hinge zones of the intrafolial folds (F_1) an earlier phase of the mylonitic fabric (S_{1a}) was folded before being transposed in the dominant fabric (S_{1b}). Thus, the main foliation is a composite fabric herein called $S_{1a,b}$ or S_1 for short (Fig. 7a). S_1 contains a well-developed mineral lineation or rodding lineation, L_{1x}, which typically pitches steeply to the southwest (251/55, azimuth/plunge; Fig. 6a, b). L_{1x} is defined by the oriented growth of plagioclase aggregates, hornblende and scapolite in calc-silicate and amphibolite units, by biotite and sillimanite in biotite schist, and by quartz-feldspar-rodding in more felsic units and quartzite. F_1 intrafolial folds have fold axes that are close to parallel to L_{1x}, and sheath-folds have been observed outside the pit.

In the quartzo-feldspathic units in the main ore zone, the S_1 foliation intensifies to a mm-scale lenticular to laminar fabric characteristic of mylonite (Fig. 4g). This fabric has been largely annealed resulting in a granular texture in thin section, characterized by alternating ribbon grains of quartz and plagioclase (Fig. 5e). Within the present geometry, trails of rotated boudin blocks of coarse-grained black quartzite layers within calc-silicate, exposed in the north wall of the pit, are consistent with a normal west-down shear sense, but otherwise shear sense indicators (asymmetric clasts, S-C fabrics, shear bands etc.) are lacking.

Across the pit the orientation of S_1 varies around two principal groupings: 300/60 and 260/55 (Fig. 6). In the western half of the pit, S_1 dips to the west-northwest (300/60), whilst in the eastern half of the pit, S_1 dips due to the west or south-southwest with S_1 steepening from 55° to 70° in the southeast corner of the pit (Fig. 3a). L_{1x} does not vary greatly in orientation in either of the two domains and remains more or less constant around 250/55, which is parallel to the intersection line between the various S_1 orientations (Fig. 6b). An abrupt change in orientation of the S_1 foliation occurs in the center of the pit where it can be mapped as a foliation truncation plane. This truncation plane originated during D_1, but it was reactivated as a brittle-ductile shear zone during D_3 and it is now characterized by an intensely foliated biotite-chlorite-schist zone as discussed below. The north to north-northeast trending foliation truncation plane dips ~55° to the west and connects the hanging wall quartzite in the southern wall of the pit to the footwall quartzite in the north (Fig. 3a). It more-or-less coincides with the ore zone (Fig. 6). Within the open pit, S_1 orientations also vary around quartzite boudins and along 10 m scale northwest-trending shear-band-like high strain zones that locally cross the main foliation (e.g. in the upper benches in the southeast corner of the pit).

Peak-metamorphic conditions in Tick Hill pit were reached during D_1 shearing and folding (e.g. Choy, 1994). The grade of metamorphism during D_1 reached upper-amphibolite to granulite facies as indicated by the ductile behavior of K-feldspar and plagioclase in sheared quartz-

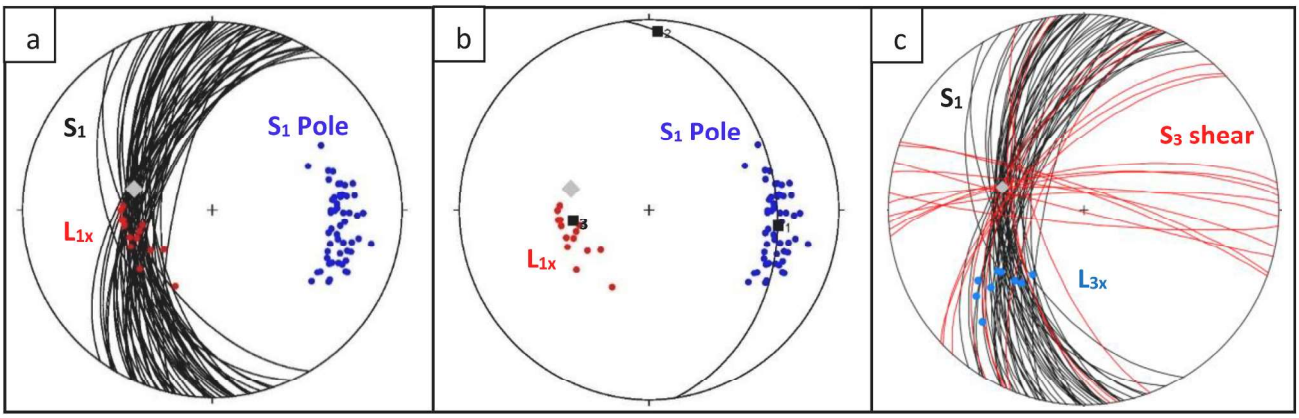


Fig. 6. Orientation data for structural elements visible in the pit at Tick Hill: (a) Great circles = S_1; blue dots = poles to S_1; red dots = L_{1x}; grey diamond = long axis of 16.5 g/t Au ore envelope; (b) Shown is the best fit great circle through the poles to S_1. Note this great circle has a pole (3) that coincides with L_{1x}; (c) Black great circles = S_1; red great circles = S_3 shear zones and normal faults; blue dots = L_{3x}; grey diamond = long axis of 16.5 g/t Au ore envelope.

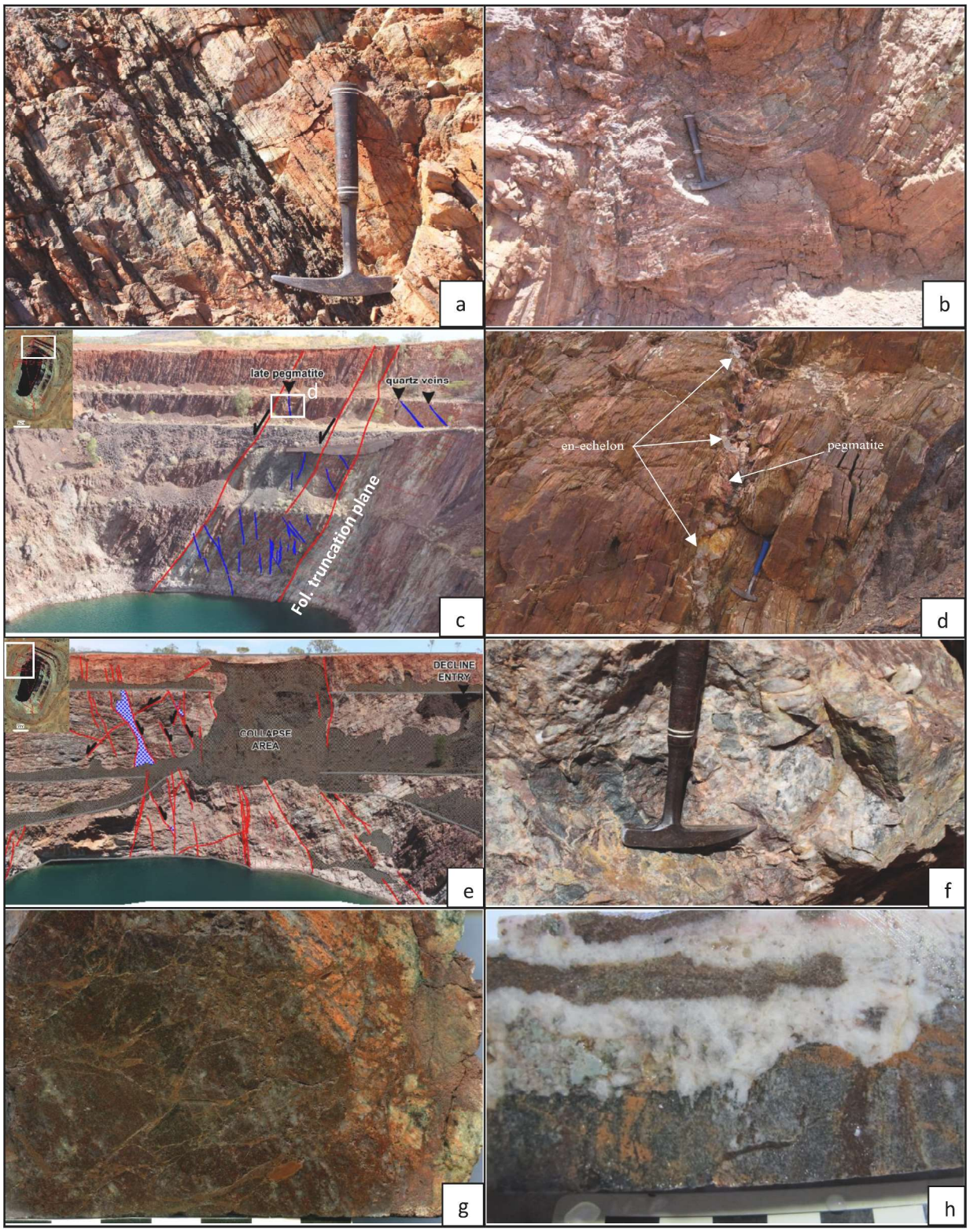


Fig. 7. Representative D_{1-4} structures and alteration textures: (a) S_1 fabric in gneissic calc-silicate intercalated with biotite schist bands in the north wall of the pit; (b) Upright folds in the north wall of the pit interpreted as D_2 vergence folds; (c) North pit wall, showing the D_1 foliation plane reactivated as a D_3 shear zone (red). En-echelon D_3 pegmatite and quartz veins (blue) are indicative of sinistral-normal movement on the shear zone during D_3; (d) Close-up of syn-D_3 pegmatite containing en-echelon quartz veins in (c) that indicate a normal shear sense; (e) East-trending, D_3 normal faults (red), some with breccia (blue) in the northwest corner of the pit; (f) D_3 brecciated and altered calcsilicate gneiss with trace sulphides; (g) High-grade calc-silicate breccia in the ore zone, which is associated with D_3 sheeted veins and quartz-feldspar-chlorite-hematite alteration; (h) D_4 veins with calc-silicate breccia fragments consisting of quartz, carbonate and green clay minerals that overprint the late D_3 red rock alteration.

feldspar mylonite, intense ductile folding (including sheath folding) in amphibolite, the presence of coarse-grained metamorphic pyroxene in leucocratic segregations within amphibolite, and hornblende-pyroxene and sillimanite assemblages defining the S_1-L_1 fabrics. In addition, garnet-hornblende-pyroxene-plagioclase-quartz assemblages in amphibolite gneiss were encountered in drill core 800 m north of the pit. The D_1 deformation features in Tick Hill pit correlate with regional D_1 deformation events described in the southern MKD (e.g. Blake and Steward, 1992; Passchier, 1992; Rutherford, 2000).

Within the pit and surrounding areas numerous quartzo-feldspathic granitic bodies occur that are variably deformed. Many are strongly mylonitic and fine-grained throughout, whereas others preserve less deformed cores with mylonitic rims. The quartzo-feldspathic units were described as the intrusive Tick Hill Complex (Wyborn, 1997) and have been interpreted as granite intrusions that were emplaced syn-tectonically at various times during the development of S_1 (Le et al., 2021).

3.2.2. D_2 events

Regional mapping shows that the Tick Hill deposit is situated in the eastern limb of a large (km-scale) synformal, D_2 structure (the Tick Hill syncline; Fig. 2b) that folds S_1 around an upright fold with an axial planar trace that parallels the regional trend of S_1. Within the pit, no clear D_2 structures are visible with the exception of rare open, near-cylindrical similar folds that occur on a 0.1–1 m scale (Fig. 7b). Such F_2 folds are invariably east-verging with near-horizontal north-trending (020) fold axes, and they contain no clear axial planar fabrics. Metamorphic conditions during D_2 are poorly constrained due to the absence of clear S_2 fabrics or mineral assemblages, but the highly ductile nature of regional D_2 folds, their transposition into the main fabric further west (Laing, 1993) and continued stability of peak assemblages within D_2 fold hinge zones suggests that conditions remained high.

3.2.3. D_3 events

D_3 in the Tick Hill pit is characterized by a network of fault zones and associated fractures and veins that accommodated normal movements and facilitated retrograde alteration (Fig. 7c–e). The S_1 foliation is locally reactivated as, or truncated by D_3 fault zones, that are characterized by a micaceous foliation and the alignment of fine-grained chlorite (after biotite) to define L_{3x} (most clearly observed in the north wall of the pit). This lineation pitches shallowly to moderately south-southwest (~230/40, Fig. 6c), and is locally paralleled by quartz striations. D_3 fault planes are associated with damage zones including breccia zones and quartz veins, some of which are arranged in an en-echelon fashion (Fig. 7c,d) consistent with a sinistral-normal sense of movement. The most conspicuous D_3 shear is exposed in the north wall of the pit as a biotite-chlorite schist zone that parallels the D_1 foliation truncation plane passing through the center of the pit. This fault zone coincides with the ore zone. A major D_3 fault zone also developed along the footwall margin of the hanging wall quartzite, and it truncates the hanging wall quartzite in the south wall of the pit (Fig. 3a).

A series of parallel, east-trending, steeply (mostly north) dipping, normal faults (Figs. 3a, 6c, 7e) developed in the northwest corner of the pit. These faults mostly do not cross the pit but appear to merge with the north-northeast-trending D_3 faults in the center of the pit, including the main D_3 fault that parallels the D_1 foliation truncation plane (Fig. 3a). The east-trending faults display dm- to m-wide, quartz-feldspar alteration haloes or rims developed on either side of individual faults, and associated albite-epidote-hematite veins.

D_3 faulting involved widespread fracturing, veining, breccia formation and quartz-feldspar alteration visible in outcrops and in drill cores. These features are concentrated in the strongly silicified core of the deposit, and the D_3 fracturing, at least in part, overprints earlier silicification. Fracture sets include thin (<2 mm wide) grey quartz veins that trend between 80 and 100° and that occur as bundles of partings along the S_1 mylonite fabric, especially in the quartz-feldspar mylonite, and drill intersections suggest that breccia is commonly associated with the sheeted veins in the lower levels of the high-grade ore zone (Figs. 3b; 7f, g).

Fracture sets also include northeast trending faults (~030°) that display sinistral displacements in drill core and are associated with albite-hematite altered quartz veins, and north- and east-trending cataclastic shatter zones best developed in silicified quartzite and schist. D_3 fractures are commonly highlighted by pink and red feldspar alteration, which also forms the matrix to shatter zones along fractures. In the ore zone (the "galahstone"), these fracture sets merge into a continuous network and many of the fractures and associated quartz veins contain visible gold. Steep east-trending fracture zones are present in all drill cores through the ore zone, and they are particularly common in gold-bearing zones. In some drill cores, the fracture zones widen to several 10 s of cm where they are characterized by chaotic fabrics and breccia. D_3 fracture zones coincide with widespread quartz-feldspar-chlorite-hematite alteration as well as locally developed carbonate alteration.

Several drill cores preserve late-stage, coarse-grained quartz-feldspar veins, which resemble the metasomatic alteration rims that decorate D_3 fractures and veins. These late tectonic quartz-feldspar zones have been interpreted as syn-D_3 metasomatic overgrowths.

3.2.4. D_4 events

D_4 structures represent the latest phase of deformation recorded in the Tick Hill pit. On the scale of the pit, D_4 involved the formation of brittle east-northeast-trending and steeply north-dipping faults (Fig. 3a) that formed in combination with steep northwest-trending secondary faults. The main east-northeast-trending fault has an apparent dextral displacement. D_4 faults displaced the quartzite units and were associated with cataclasite formation and chlorite-hematite-goethite alteration along slicken-sided fracture zones as well as open-space carbonate fill. In drill core, D_4 structures include late-stage fractures and cataclasite zones with quartz-carbonate-clay fill and associated clay alteration haloes, which overprint D_3 fractures and veins (Fig. 7h).

4. Gold mineralization and alteration at the Tick Hill deposit

As mentioned in the introduction, earlier workers at Tick Hill noted the problem that gold seemed to have a relationship to both old (D_1) and young (D_3) structures (e.g. Choy, 1994; Tedman-Jones, 2001). Gold inclusions in peak-metamorphic minerals, an alignment of gold with the S_1 fabric and a spatial association with syn-D_1 silicified deformation zones were cited as evidence for early gold (e.g. Choy, 1994). A spatial association with late-tectonic laminar quartz veins and associated chlorite-albite-hematite alteration, and the presence of gold along D_3 fractures and breccia zones were cited as evidence for a D_3 origin (e.g. Tedman-Jones, 2001). What follows is a description of gold distribution patterns and associated mineral assemblages in relation to the earlier and later structures. An in-depth discussion of the potential genesis of the ore body is provided in the discussion.

4.1. Ore body geometry and associated metal distribution

The ore body geometry as defined by the 1 g/t ore envelope for the Tick Hill deposit is carrot-shaped and tapers down to a vertical depth of 240 m (MIM, 1993, 2000; Tedman-Jones, 2001). The ore body dips ~55° to the west, i.e. parallel to S_1, and has a linear high-grade (i.e. 16.5 g/t) core that plunges 55° to 285 (Fig. 6). With increased depth, the strike extent of the ore zone decreases and in the two lowest mine levels (130 mRL and 117 mRL, e.g. Fig. 3b), the ore trend switches abruptly from north-northeast to east and the ore zone has been described to narrow to several meter-wide chlorite-hematite-carbonate breccia veins (Fig. 3b; Tedman-Jones, 2001).

The geochemical surface expression of the Tick Hill gold anomaly (>0.1 ppm) was about 160 × 30 m and coincided with a pre-mining,

north-northeast-trending, 210 × 50 m magnetic low (Nano et al., 2000, Fig. 8). The location of the gold anomaly that runs across the pit overlaps with a strongly D_3 fractured and hematite-altered zone in the immediate hanging wall of the D_1 foliation truncation plane that was reactivated as a D_3 shear zone (Figs. 3a, 6b). The plunge of the high-grade core of the ore body coincides with the intersection lineation between the north-northeast- and east-trending D_3 faults, and the intersection lineation between the D_3 faults and the S_1 foliation planes as measured in the pit. The plunge of the high-grade core is also close in orientation to the measured L_{1x} mineral lineation, which is somewhat variable in orientation (Figs. 3a, 6c). The low grade (i.e. 0.1 g/t) ore envelope coincides with areas where east-trending D_3 fractures and breccia zones are most prominent, and extends outside the pit along some of the more prominent east-trending D_3 fracture zones.

Gold mineralization is largely confined to the strongly altered quartz-feldspar mylonite sub-unit and adjacent biotite schist, calcsilicate, and hanging wall quartzite (Fig. 3). The historical assay data shows that the boundaries to the mineralization are sharp as grades drop abruptly away from the $D_{1\text{-}2}$ silificied and D_3 altered fracture zones.

In drill cores and thin sections, gold can be commonly seen as an alignment of coarse grains that parallel the dominant mylonitic S_1 fabric. Gold grains also commonly occur associated with thin laminar quartz veins of D_3 origin, which either occur along the S_1 mylonitic foliation or along steep east-trending fractures. Mineralization shows a spatial relationship with D_3 alteration haloes near post-tectonic coarse-grained quartz-feldspar dykes, and fine gold grains typically occur near patches of chlorite, albite and hematite. The east-trending quartz-feldspar veins are locally associated with breccia zones, which in drill core are most prominent at depth in the immediate footwall of high-grade ore zones (Fig. 7f,g). At shallower levels where breccia is less common, high-grade mineralization is concentrated in areas of intense laminar D_3 veining (e.g. Figs. 4g, 9a-b).

Gold occurs almost exclusively as disseminated grains of free gold up to 0.5 mm in size with Au/Ag ratios of >100. The quartz-feldspar mylonite is locally extremely gold-rich (e.g. up to 3209 ppm @ 0.5 m in DH TH014), and gold grains locally display a characteristic granoblastic texture (Fig. 9c). Within the high-grade ore zones, gold grains commonly display bimodal grainsize distributions with irregularly shaped larger grains surrounded by a halo of finer grains (e.g. Choy, 1994; Fig. 9d,e). A few of these finer grains contain small amounts of Ag (<5.3 wt%) and Cu (<2 wt%). Coarse-grained gold is commonly enclosed within recrystallized quartz, with quartz appearing as a

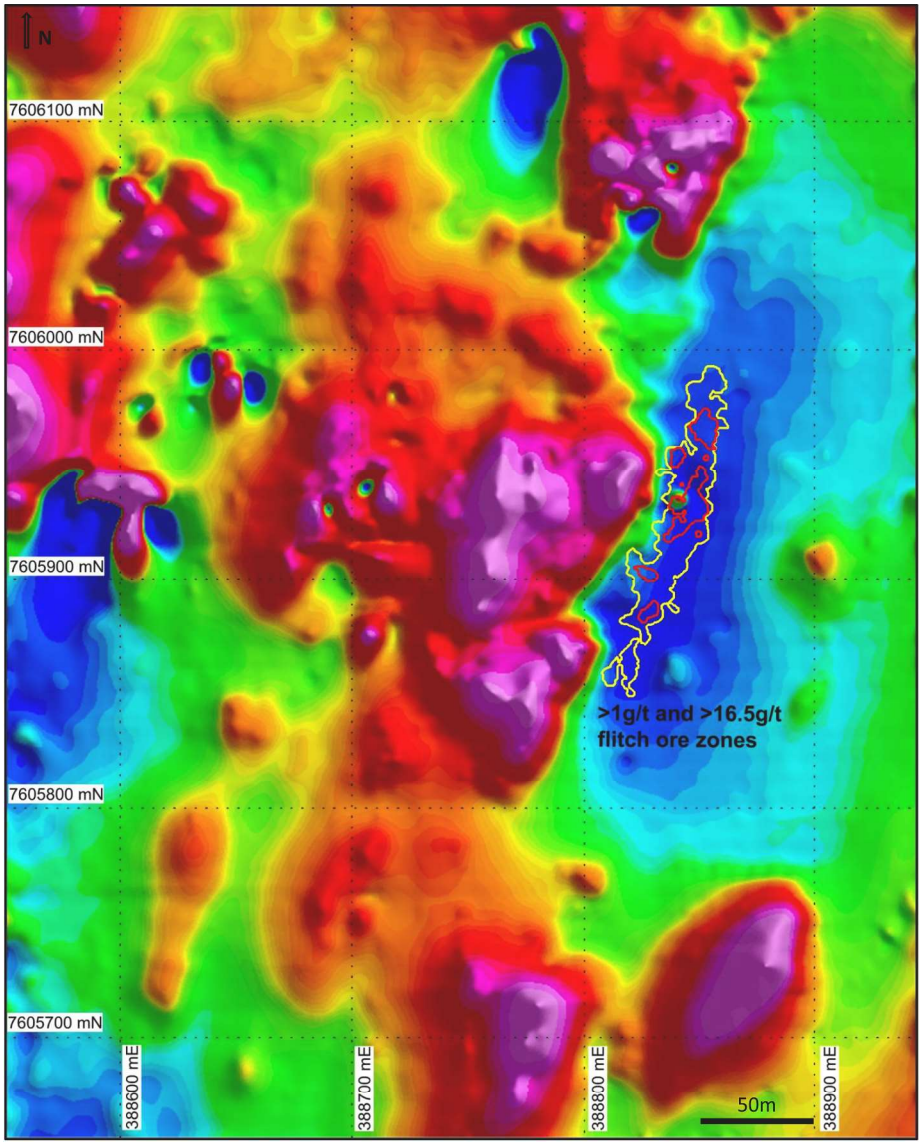


Fig. 8. Ground magnetic map of the Tick Hill area, overlain with Au grade contours, illustrating the coincidence of gold mineralization with an area of magnetic depletion (reproduced from Nano et al., 2000).

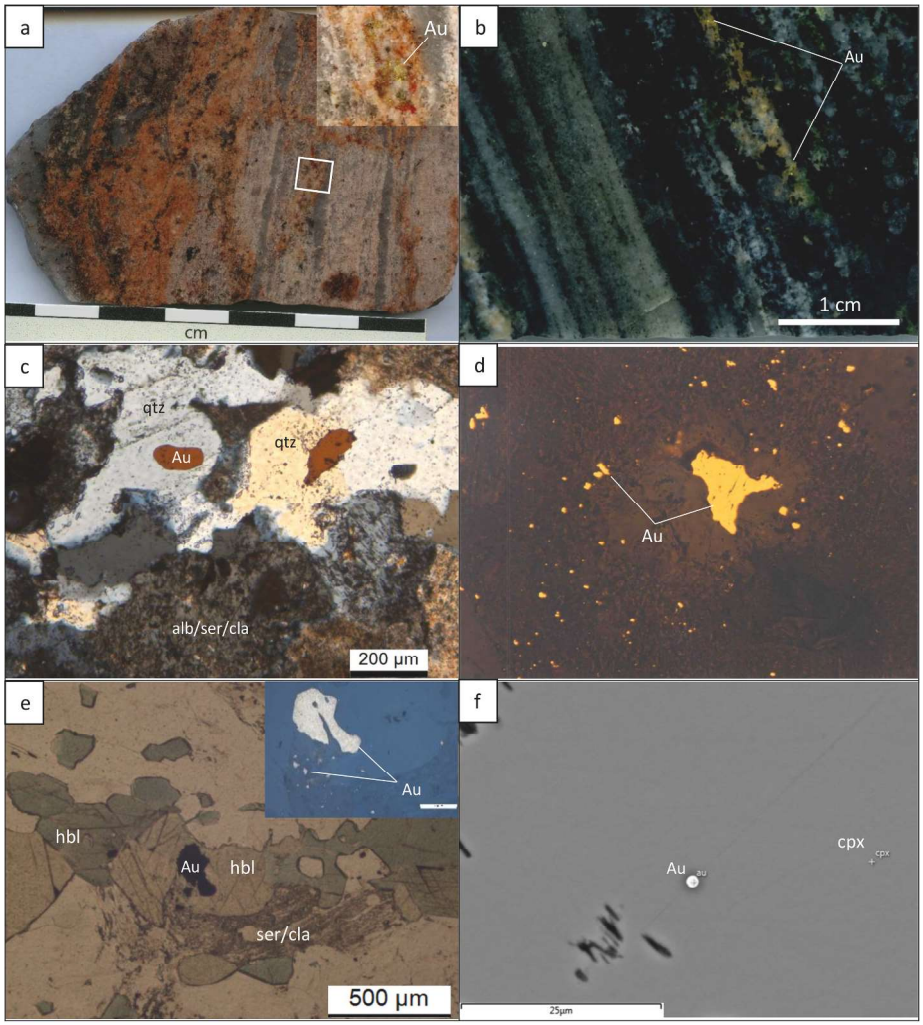


Fig. 9. Examples of textures associated with gold mineralization: (a) Gold-rich metasomatized quartz-feldspar mylonite, a close-up of the white box is shown in the top right; (b) Gold mineralization concentrated along feldspar-rich selvages in strongly foliated amphibole-rich calc-silicate; (c) close-up of coarse-grained gold grains in (a). Gold (Au) is commonly contained within quartz (qtz) or surrounded by a moat of quartz in recrystallized quartz-feldspar mylonite in which albite (alb) is replaced by late-D_3 sericite (ser) and clay minerals (cla); (d) Microphotograph showing a coarse grain of gold with a halo of finer gold grains suggesting local dissolution and remobilization of early stage gold (image after Choy, 1994); (e) Microphotograph showing coarse-grained gold within peak-metamorphic (D_1) hornblende (hbl), while fine-grained gold occurs along grain boundaries where it is associated with sericite (ser) and clay (cla) alteration (after feldspar). A close-up of the Au grains under reflected light is shown in the top right; (f) An SEM image showing a gold inclusion hosted within peak-metamorphic clinopyroxene (cpx) in amphibole-rich calc-silicate.

metamorphic moat around the gold. Gold also occurs along the grain boundaries between quartz and feldspar grains. Within calc-silicate units, gold is locally enclosed within granoblastic scapolite, hornblende and pyroxene grains that are aligned in the peak-metamorphic S_1 fabric (e.g. Fig. 9b,e,f). Fine-grained gold occurs either as haloes near larger gold grains or as trails associated with strongly silicified zones and alteration minerals that included bismuth selenides and sulfides (Table 2). In general, the sulfide content in the mineralized quartz-feldspar mylonite unit is less than in the other units, and the abundance of sulfides increases towards the footwall of the deposit.

The high-grade core of the Tick Hill deposit shows only minor enrichment in other metals, and sulfides. Available assay data for a restricted number of elements (Cu, Co, Ni, Pb, Zn, As, Fe, Mn) from exploration holes drilled in the 1990s (MIM, 2000) indicate that with few exceptions, on a meter-scale, gold values show no correlation with any of the other metals. On the scale of the deposit, a general enrichment in Cu (>100 ppm), Co (>40 ppm), S, As, and Bi has been suggested for the immediate footwall of the ore zone (Nano, 1999; Tedman-Jones, 2001), with minor Co enrichment (>40 ppm) partly overlapping with the 1 g/t Au envelope. Cu values reach up to several 1000 ppm in the footwall to the ore zone and can be linked to chalcopyrite-pyrite and minor bornite-pyrrhotite mineralization, which is possibly also responsible for an induced polarization anomaly that was observed over the Tick Hill ore body (Nano, 1999). Cu values are rarely high in the ore zone itself. At a larger scale, it is clear that Cu and Co anomalies are not restricted to the vicinity of the ore zone, but also occur in the hanging wall of the ore zone, where Cu values locally reach 100′s ppm away from mineralization and alteration (Fig. 10). In general Cu shows moderate to strong correlations with Co and Ni and a spatial relationship with amphibole-rich lithologies.

4.2. *The spatial distribution of the alteration halo around gold mineralization*

The Tick Hill deposit is associated with two periods of alteration: a first that occurred at high temperatures during D_1, and a second that occurred at lower temperatures during D_3. Early high temperature alteration involved the emplacement of gold that was incorporated in hornblende and diopside grains aligned in the S_1 fabric. Evidence for this early event is only partly preserved, because of the intensity of the later stages of hydrothermal overprints during D_3, and the exact spatial distribution of the early alteration halo is uncertain.

The early alteration event is characterized by intense silicification and associated magnetite alteration that is most evident within the hanging wall quartzite unit (Fig. 4c). Within the ore zone, syn-D_1 silicification was intense and involved the growth of quartz at the expense of other silicate phases (Fig. 11a), which now occur as inclusion trails in quartz. Early magnetite was largely destroyed by the lower temperature D_3 hydrothermal overprint during which magnetite was replaced by hematite (Fig. 5c). Gold grades in drill core display a negative correlation with magnetic susceptibility, and this effect is visible on a larger scale by the presence of an aeromagnetic low that coincides with the ore zone and the D_3 alteration halo (Fig. 8).

The D_3 alteration events resulted in the formation of a low- to

Table 2
Late (syn D_{3-4}) hydrothermal mineral assemblages and paragenesic stages for the ore zone at Tick Hill. Cg = coarse grain, Fg = fine grain.

Minerals/ Deformation events	*D_3*					*D_4*
	Stage 1	*Stage 2*	*Stage 3*	*Stage 4*	*Stage 5*	*Stage 6*
Quartz						
Albite						
Oligoclase						
K-feldspar						
Hornblende						
Actinolite						
$Chlorite_1$						
$Chlorite_2$						
$Chlorite_3$						
Epidote						
Sericite						
Clay minerals (smectite-illite)						
Calcite						
Magnetite						
Hematite						
Leucoxene						
Gold (Cg matrix)						
Gold (Fg matrix)						
Gold (Fractures)						
Chalcopyrite						
Bornite						
Cobaltpentlandite? (Ni-Co-Cu-S±Fe)						
Pyrrhotite						
$Pyrite_1$						
$Pyrite_2$						
Pyrite (undifferentiated)						
Guanajuatite, Bi_2Se_3						
Junoite, $Pb_3Cu_2Bi_8(S,Se)_{16}$						
Cerromojonite; $CuPbBiSe_3$						
Molybdomenite; $PbSeO_3$						

Quantity: Dominant — *Trace*

moderate-temperature alteration zone that is about 100 m in diameter and overprinted the earlier high temperature alteration assemblages as well as the D_1 peak metamorphic mineral assemblages and associated structures (Figs. 3, 10, 11a). This later alteration is most prominently developed in the ore zone and hanging wall rocks to the ore zone above the S_{1-3} foliation truncation plane, whilst the footwall rocks to that surface are significantly less altered (Geological Survey of Queensland, 2015).

The lower temperature alteration assemblages vary with rock type and display a zonal pattern, with most intense alteration occurring along D_3 fracture zones and associated breccia. From the proximal mineralization outward, the alteration zonation includes (Fig. 10): (1) intense to (2) strong silicification and associated growth of abite-hematite-chlorite-epidote-sericite-actinolite/hornblende-oligoclase (Fig. 11), surrounded by (3) a shell characterized by chlorite and epidote (Fig. 11b), and (4) an extensive zone with clay alteration. Zonal

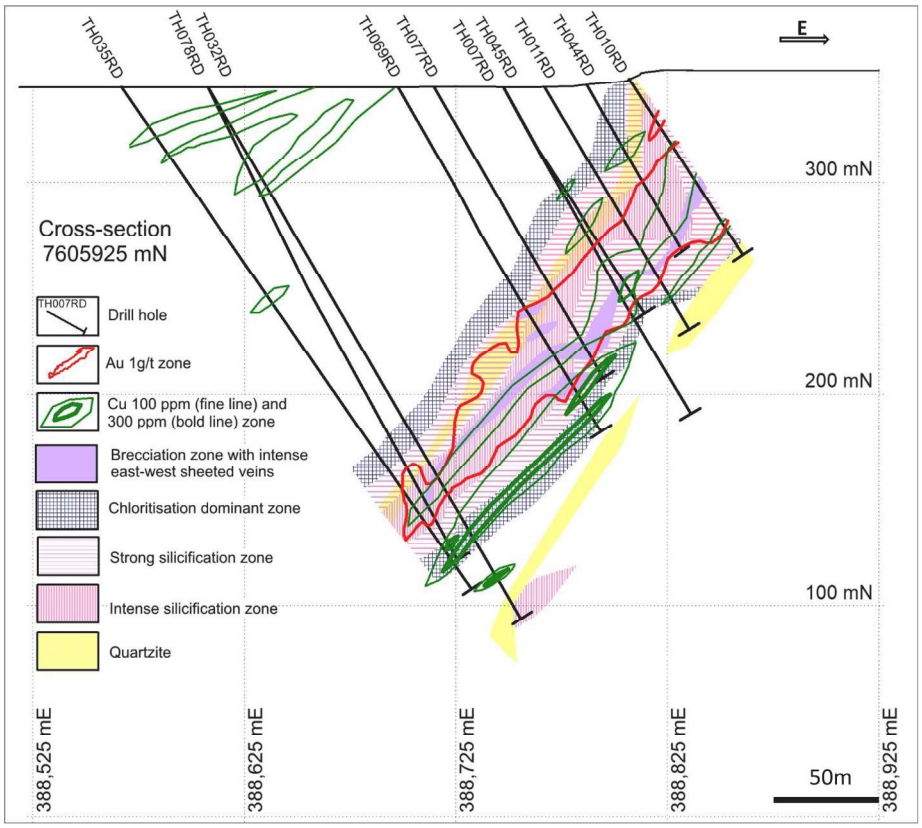


Fig. 10. Cross-section 7,605,925 mN showing the spatial relationship between various alteration zones, brecciation, 100–300 ppm Cu zone and the 1 g/t ore envelope at Tick Hill based on core logging and assay data.

boundaries are gradational with localized overlaps in alteration assemblages, whilst late clay alteration occurs throughout (e.g. Geological Survey of Queensland, 2015, Appendix 1).

Within the high-grade ore zone, intense silicification affected the quartz-feldspar mylonite and biotite-rich schist (Fig. 11a). Here, pervasive silicification with quartz growth across the mylonitic fabric occurred early (i.e. pre- or early-D_3), with later silicification linked to the emplacement of thin quartz veins (sub-) parallel to the S_1 foliation, and the growth of quartz in alteration haloes near quartz-feldspar veins and pegmatite dykes.

Carbonate alteration generally occurs as a late-D_3 and D_4 fracture fill. In the mineralized zone, calcite locally occurs as secondary growth along sheeted quartz veins and east-trending fractures, but carbonate growth is not pervasive. However, in the keel of the deposit in the lower levels of the mine, gold was mined from east-trending breccia veins that were reported to contain chlorite-hematite-carbonate in the matrix (Tedman-Jones, 2001), i.e. at depth carbonate growth may have been more abundant and it occurred in associated with gold, although we could not confirm this in drill core.

4.3. Paragenetic sequence

Most hydrothermal alteration minerals associated with gold mineralization formed during D_3. However, there is clear textural evidence that gold was present during D_1 peak metamorphism when the main gneissic fabric formed and an early stage of high temperature alteration occurred (Table 1; Fig. 9e,f). The main minerals that characterize early, high temperature alteration are magnetite and quartz, which are best preserved in the hanging wall quartzite unit, where quartz and magnetite largely replaced biotite, feldspar, and in places amphibole (e.g. Geological Survey of Queensland, 2015), which are now only visible as trails of largely resorbed grains aligned along S_1 and included in granoblastic quartz. The magnetite content in the hanging wall quartzite increases upwards and grades into a near-massive magnetite zone towards the upper contact of the quartzite, where magnetite is aligned with S_1 and inter-grown with syn-D_1 high-temperature minerals including scapolite and hornblende, suggesting that much of it formed pre- or syn-D_1 (Table 1). Considering that the early magnetite-quartz alteration is prominent in the hanging wall of the high-grade ore zone, and magnetite within the ore zone itself was largely replaced by D_3 hematite (Fig. 8), it is likely that early magnetite alteration was associated with deposition of early gold.

The best evidence for early gold mineralization can be found in mineralized amphibolite-rich, calc-silicate gneiss horizons, where gold inclusions occur in peak-metamorphic scapolite, hornblende and diopside grains that were unaffected by later retrograde alteration (e.g. Fig. 9f). There are no obvious micro-fractures in the scapolite, clinopyroxene or hornblende grains that could indicate later remobilization of gold, and the presence of these inclusions indicates that gold was present when the S_1 fabric formed. The presence of early gold is further supported by its bimodal grainsize distribution in some high-grade ore zones, where coarse gold grains that are typically aligned in the S_1 fabric and surrounded by a halo of fine gold (Fig. 9d,e; Choy, 1994).

Emplacement of early gold may have been associated with the deposition of sulfides. Texturally early D_1 chalcopyrite has been observed as inclusions inside amphibole, which itself occurs as inclusions inside coarse-grained, peak-metamorphic, almandine garnet (e.g. in drill core TH99, 800 m north of Tick Hill; Le, 2021). Away from the main ore zone, chalcopyrite and pyrite are relatively common in amphibolite gneiss, where the sulfides occur along S_1 foliation traces. Thus, a first stage of gold mineralization occurred in association with the peak-metamorphic assemblage and an early stage of magnetite-quartz alteration when chalcopyrite was present within the system (Table 1).

The most obvious alteration assemblages visible in the Tick Hill pit

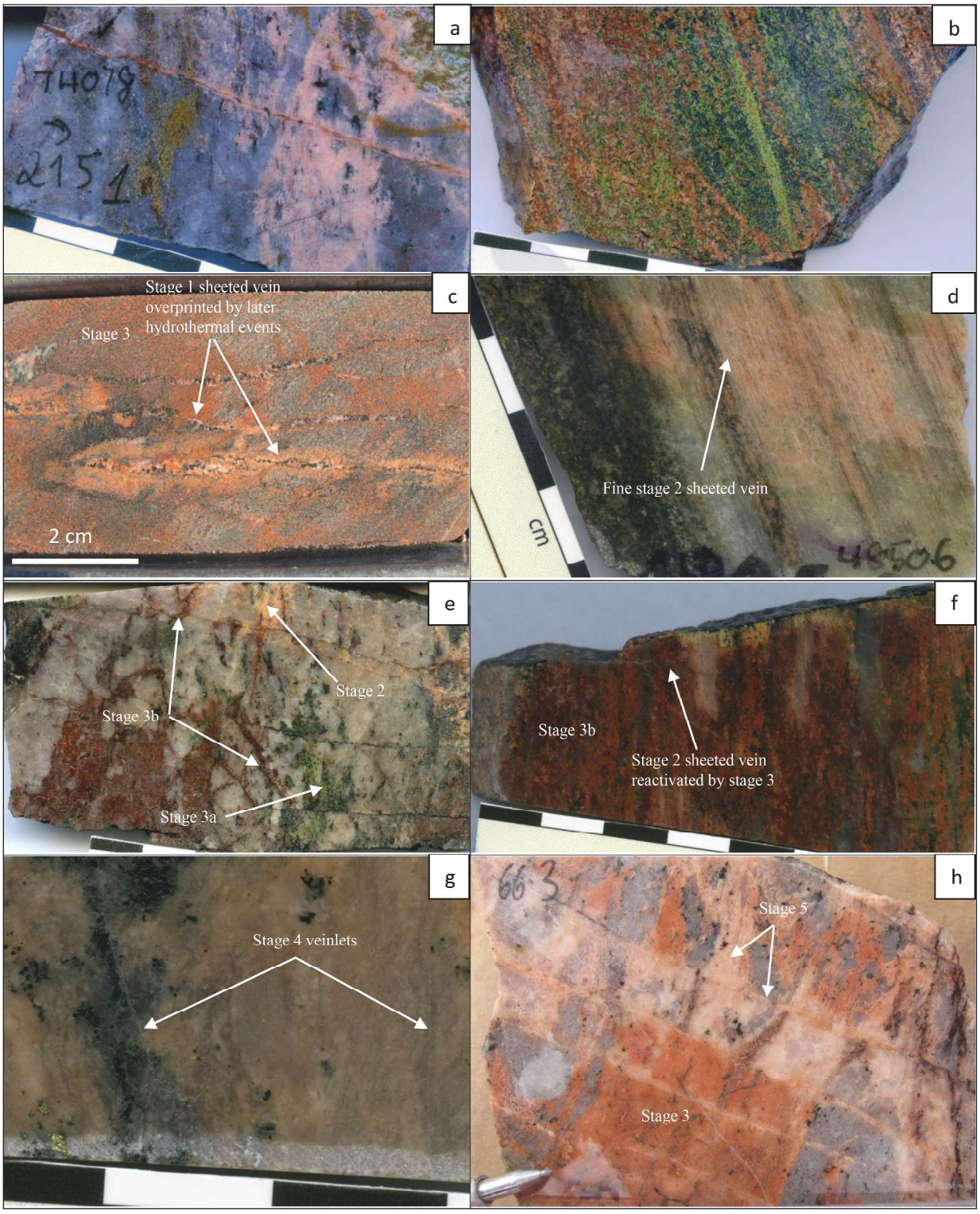


Fig. 11. Examples of alteration assemblages in drill core from the high-grade ore zone, reflecting the paragenetic stages recognised in Tick Hill: (a) A cm-scale image of the $D_{1\text{-}2}$ silicification zone, with relic biotite, overprinted by D_3 pink feldspar-quartz alteration and gold mineralization in the sheeted veins in the center of the image; (b) A cm-scale image of D_3 chlorite-epidote alteration in the hanging wall to mineralization. (c) Stage 1 east-trending sheeted veins comprised of quartz, feldspar and magnetite, which were overprinted by stage 3 red rock alteration. (d) Stage 2, east-trending, finely laminated, sheeted veinlets and associated pink feldspar-quartz alteration haloes overprinting the S_1 fabric. Many of the fine veins parallel the mylontic fabric and resemble quartz-ribbon grains, thus masking their abundance. (e) High-grade gold mineralization in intensely silicified biotite schist, associated with east-trending, stage 2 sheeted quartz-feldspar veins (pink), and overprinted by stage 3a chlorite-epidote and stage 3b hematite-rich alteration (red rock alteration). (f) Stage 3 red rock alteration affecting silicified biotite schist with stage 2 sheeted veins. (g) Stage 4 veinlets of calcite overprinting earlier amphibole and quartz-feldspar alteration. (h) Stage 5 light pink feldspar along thin veins that overprint stage 3 red rock alteration.

today formed during D_3 and D_4, and involved six hydrothermal stages (Table 2). During stage 1, magnetite-bearing feldspar veins were emplaced associated with the formation of an alteration assemblage (stage 1) that included quartz-albite (±oligioclase)-hornblende-magnetite-hematite (±leucoxene). This was followed by at least three stages during which gold was either introduced or remobilized, with hematite and chlorite being the most characteristic alteration minerals in outcrop. Stage 2 coincided with the main period of gold mobility, and involved quartz-feldspar veining and alteration characterized by the growth of quartz-albite-actinolite-chlorite$_1$-hematite (±leucoxene) progressing into stage 3 with the growth of K-feldspar-sericite-chlorite$_2$-epidote-hematite (stage 3a) followed by hematite, smectite and illite (stage 3b). Stage 4 is characterized by minor calcite veining, late chlorite$_3$ growth and the remobilization of some gold along fractures. Stage 5 events postdated mineralization and included late-D_3, pale pink quartz-albite flooding and the renewed growth of magnetite along isolated fractures. During later D_4 events additional quartz-carbonate-clay alteration (stage 6) occurred along late faults, with no evidence that gold was remobilized. The paragenetic sequence and mineral assemblages that formed during each of these six stages are discussed in more detail below and presented in Table 2.

The early-D_3 emplacement of ***stage 1*** feldspar veins marked the onset of younger hydrothermal alteration events that predated the introduction of gold during D_3, or the re-mobilisation of early gold that had formed during D_1. Most veins of this type are steep, have an east trend (Fig. 11c), and they contain magnetite and titanite. They represent the earliest set of veins that form part of the family of laminar, sheeted veins that characterize the ore zone. They are common in the hanging wall sequence, and their occurrence in the footwall sequences is uncertain, due to a paucity of available drill core. Vein emplacement was associated with the formation of a mineral assemblage (stage 1) that included quartz-albite-oligioclase-hornblende-magnetite-hematite (±leucoxene). Intense albite alteration characterized stage 1 and occurred with the formation of oligoclase, hematite and hornblende. Stage 1 magnesio-hornblende (Mg/Mg + Fe = ~0.6, minor Na_2O, K_2O, Cl, and TiO_2) is blue-green in colour (Fig. 12a), and either replaced older D_1 hornblende, or occurs as clots overgrowing the dominant fabric.

During ***stage 2***, numerous feldspar-rich veins were emplaced that either contain gold, or that were associated with alteration haloes that contain gold (Fig. 11d–f). These veins include thin (<1 mm), east-trending, laminar veins, and north-trending veins that can be up to 10 cm wide and parallel the S_1 foliation. The stage 2 veins are best developed as feldspar-filled fractures within the silicified biotite-rich schist, in quartz-feldspar mylonite and in the hanging wall quartzite (Fig. 11d–e). Stage 2 veins consist of pale pink to dark pink feldspar and quartz. The pale pink feldspar is commonly albite with lesser oligioclase, while the darker pink feldspar is either albite or oligoclase with abundant fine-grained hematite inclusions. Overprinting relationships between veins in some drill cores suggest that stage 2 veining commenced with feldspar-rich veins and continued with the emplacement of progressively more silica-rich veins.

Stage 2 veins are associated with extensive feldspar alteration haloes that emanate from the veins, and overgrow and replace the older S_1 fabric (e.g. Fig. 11d). Alteration textures vary in intensity and include: (a) albite (±oligoclase) replacement with minor quartz that obliterated the older fabric, (b) albite-quartz alteration along thin lamellae that generally parallel the S_1 fabric, and (c) replacement alteration along networks of fine fractures that resulted in a spotted and veined alteration texture (Fig. 11e). Most gold observed in thin sections occurs in spatial association or is inter-grown with stage 2 alteration assemblages, and it commonly occurs as inclusions within granoblastic, grey quartz grains (Fig. 9c). The mineralization was associated with the growth of albite-hematite-actinolite-chlorite$_1$ and later K-feldspar-sericite (Fig. 12a–f). Intense albite alteration with oligoclase occurred early during stage 2, and became weaker towards stage 3, as K-feldspar started to develop. In general, K-feldspar formed after albite, and locally appears as reaction rims on albite grains (Fig. 12d). K-feldspar is commonly hematite-dusted, and together with hematite-dusted albite forms the red-pink feldspar alteration that characterizes stage 2 alteration zones.

Stage 2 sericite alteration is common in the mineralized zone and replaced earlier albite and oligoclase (Figs. 9c, 12a). The intensity of sericite alteration varies with proximity to stage 2 veining and is commonly associated with hematite, fine-grained gold, and minor pyrite$_1$ and chalcopyrite. Hematite formed as fine inclusions in feldspar, as grains replacing magnetite and as individual grains (Fig. 12g). Hematite commonly contains some titanium and it is intergrown with leucoxene. Stage 2 chlorite$_1$ replaced peak-metamorphic $D_{1\text{-}2}$ biotite (Fig. 12b,c), and consists of relatively Fe-rich (~30–35% FeO_{total}) ripidolite to pycnochlorite. It is characterized by a relatively high Al_2O_3 (>18.5 wt%) and minor MnO (0.1–1.3 wt%) and TiO_2 (<0.2 wt%) contents. Stage 2 actinolite is restricted to retrograde rims of stage 1 hornblende (Fig. 12a).

Within the ore zone, sulfide minerals are relatively rare, and they typically exhibit irregular, resorbed grain shapes of intergrown pyrite, pyrrhotite and chalcopyrite, with rare bornite, chalcocite, arsenopyrite, and unspecified Ni-Co-Cu-(±Fe) sulfides (possibly cobaltpentlandite) that formed during stage 2. Apart from the sulfides, fine gold grains are commonly associated with stage 2 and stage 3 Bi-selenides (e.g. Guanajuatite, Bi_2Se_3), which in many places are more common than sulfide. Where pyrite is present, texturally early stage 2 pyrite$_1$ is commonly Ni-rich, and overgrown by late stage 2-stage 3 Se (±As)-rich pyrite$_2$ and Se-rich pyrrhotite.

Stage 3 alteration is a progression of stage 2 and involved widespread green–blue chlorite$_2$-epidote alteration (stage 3a, Fig. 11e) followed by pervasive clay-hematite alteration that overprints the earlier assemblages (stage 3b, Fig. 11e–f). The intensity of this alteration as seen in drill core is related to the fracture density and the lithological composition, and, more specifically, the amount of primary ($D_{1\text{-}2}$ and early D_3) plagioclase and magnetite. Stage 3 alteration is associated with gold, which could have been either remobilized from earlier gold or newly introduced. Distal alteration minerals include illite and smectite (Appendix 1; Geological Survey of Queensland, 2015), hematite, and leucoxene (after magnetite). Stage 3, chlorite$_2$ formed in spatial associated with gold (Fig. 12e) and in the chlorite$_2$-epidote shell surrounding the ore zone. Chlorite$_2$ mostly forms non-orientated clots and is commonly intergrown with epidote, and both minerals have irregular (partly resorbed) grain shapes (Fig. 12f). Chlorite$_2$ is relatively Fe-rich (~25–30% FeO_{total}) brunsvigite to diabantite with intermediate Al_2O_3 (14–19 wt%) and minor MnO (<0.25 wt%), and TiO_2 (<0.2 wt%) contents.

Stage 4 alteration is characterized by the formation of micro-veins of calcite-quartz ± chlorite$_3$ that cut across the S_1 fabric (Fig. 11g), as well as the continued formation of clay minerals. It is important to note that such veinlets are relatively uncommon, and carbonate growth during stage 4 is not pervasive. Stage 4 chlorite$_3$ is locally intergrown with calcite, and consists of Fe-poor (~10–35% FeO_{total}) diabantite to penninite characterized by a low Al_2O_3 (13–14 wt%) content and no MnO or TiO_2. Stage 4 veins are associated with the deposition of minor gold, bismuth selenide, chalcopyrite (Fig. 12h), pyrite and rare Cu-Pb-Bi selenides that resemble junoite ($Pb_3Cu_2Bi_8(S,Se)_{16}$), cerromojonite ($CuPbBiSe_3$) and clausthalite (PbSe). Stage 4 calcite is generally pure $CaCO_3$, but occasionally contains up to 0.5 wt% MnO.

Stage 5 alteration postdates mineralization and involved the localized growth of late-D_3, pale pink feldspar and minor quartz, magnetite, specularite, and titanite (Fig. 11h). Feldspar alteration is concentrated along fracture zones that vary in width from a few decimeters to over 20 m, and it resulted in the formation of vein- or dyke-like features (Fig. 11h). These are common in both hanging wall and footwall sequences. Assay values from drill core indicate that stage 5 feldspar veins and dykes do not contain gold, and where stage 5 veins intersect mineralization, gold was depleted.

The youngest hydrothermal event at Tick Hill, defined as ***Stage 6***,

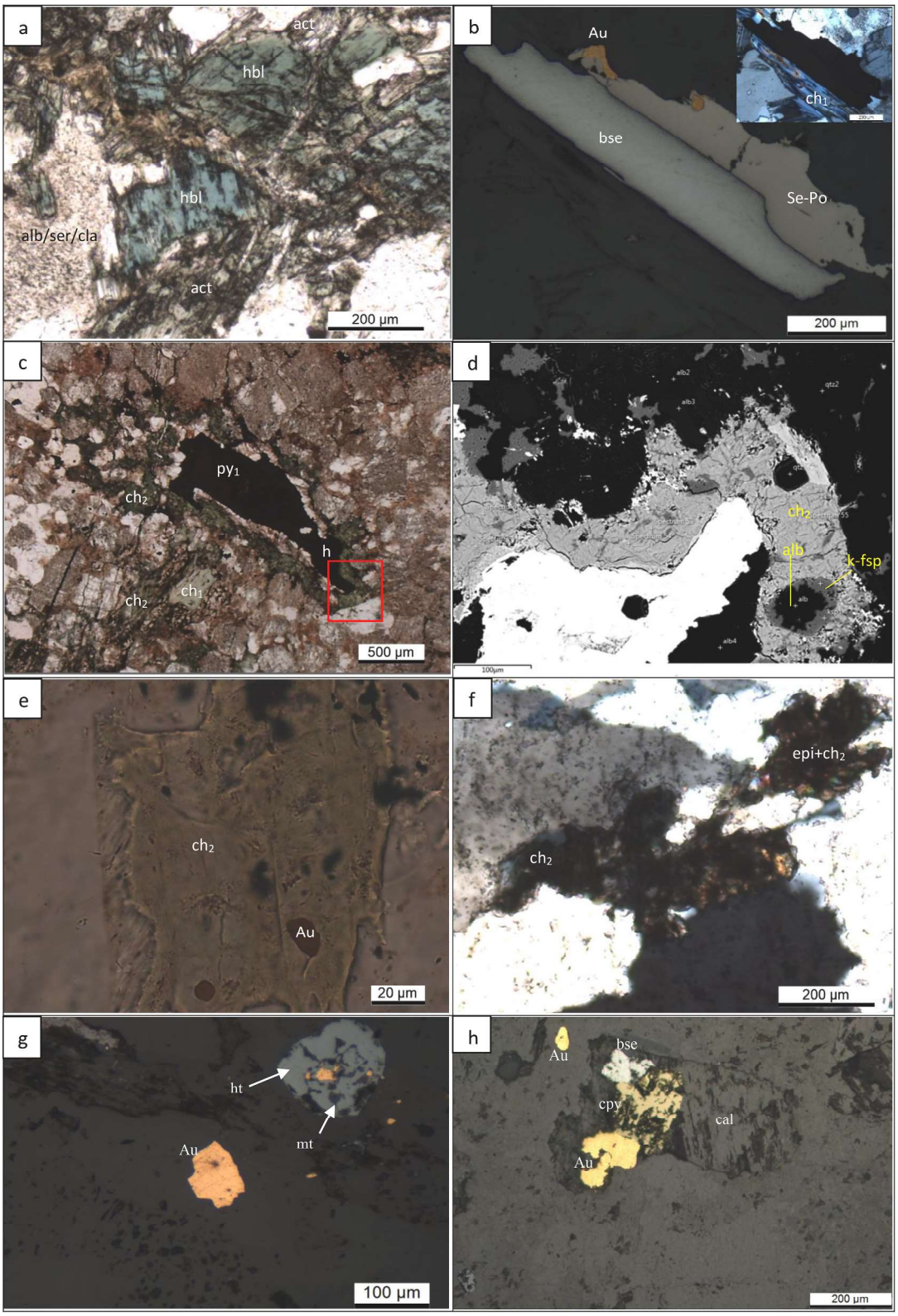


Fig. 12. Thin section and SEM images of alteration assemblages associated with gold: (a) Stage 2 actinolite (act) rimmed and replaced stage 1 hornblende (hbl) that formed along micro veins, with stage 3 sericite (ser) and clay minerals (cla) replacing stage 1 and 2 albite (alb). (b) Stage 2 chlorite$_1$ (ch$_1$) replacing earlier biotite and was associated with gold, bismuth selenide (bse) and Se-pyrrhotite (Se-Po). (c) Zoned coronal reaction rim of stage 3 green chlorite (ch$_2$), albite and quartz around an early coarse-grained pyrite (py$_1$). The matrix assemblage preserves earlier, stage 2 chlorite$_1$ (ch$_1$); the red box shows the area shown in (d). (d) SEM image showing more details of the reaction textures in (c) with early stage 3 albite (alb) inter-grown with chlorite$_2$ (ch$_2$) being replaced by later stage 3 K-feldspar (k-fsp). (e) Inclusion of fine-grained gold inside stage 3, chlorite$_2$ (ch$_2$). (f) Stage 3, chlorite$_2$ (ch$_2$) intergrown with epidote (epi). (g) Reflected light image of gold associated with stage 2 and 3 hematite (ht) after stage 1 magnetite (mt). (h) Stage 4 gold, chalcopyrite (cpy) and bismuth selenide (bse) intergrown with calcite (cal).

involved the formation of carbonate-quartz-clay assemblages along late veins and D_4 faults (Fig. 7h). In drill core, stage 6 alteration occurs in both footwall and hanging wall sequences. The veins commonly constitute infill along fault breccia with vuggy quartz, calcite, green clay minerals and minor pyrite.

5. Discussion

Since its discovery, intensive exploration in the region around Tick Hill has demonstrated that the deposit has no obvious extensions and, therefore, appears to be unique. What makes it different from other gold deposits in the Mt Isa Inlier is the high-grade, concentrated nature of the gold mineralization hosted in high-grade metamorphic rocks, the virtual lack of significant enrichment in other metals, the low sulfide content, and the presence of Bi-selenides. As such Tick Hill does not comfortably match the ore deposit models for either gold-rich IOCG deposits (e.g. Williams et al., 2001, 2005; Groves et al., 2010; Duncan et al., 2014) or orogenic lode gold occurrences with which Tick Hill has been compared (e.g. Goldfarb et al., 2005; Denaro et al., 2013).

In mapping the deposit and its associated structure, paragenesis and alteration assemblages a number of controlling factors have been identified that influenced how gold-bearing fluids at Tick Hill may have moved to trapping sites, and how these fluids interacted with the host rock to deposit gold. These controls include lithological and structural controls as well as the nature of the far field stress, and the potential role of intrusive activity.

One important and puzzling feature about the Tick Hill deposit is the evidence for texturally early (D_1) and late (D_3) gold, together with indications that early gold and sulfide mineralization may have been remobilized (Fig. 9), which has led to a variety of mineralization concepts in past exploration campaigns (Tedman-Jones, 2001). The implications for the timing and origin of the Tick Hill deposit will be discussed in more detail below.

When discussing the mineralization events we will make reference to early and late gold. With respect the late gold phase it is important to bear in mind that the evidence shows that gold was mobile during D_3 stages 2–4, and that early gold was remobilized. However, we cannot be certain that the late gold stage involved the introduction of new gold.

5.1. Controls on the distribution of mineralization at Tick Hill

5.1.1. Lithological controls

Mineralization at Tick Hill is not restricted to any one stratigraphic horizon, and the high-grade ore envelope transgresses different lithologies including quartzite, quartz-feldspar mylonite, calc-silicate gneiss, amphibolite and biotite schist (Fig. 3). All of these lithologies are characterized by strong-silicification that predated the main stage of mineralization. Thus, from a litho-chemical perspective there does not appear to be a single lithology (e.g., an Fe-rich lithology) that was especially conducive to the precipitation of gold, i.e. it is unlikely that chemical interaction between the host rock and a ligand carrying the gold was of great importance in trapping gold. Having said this, the lithologies in the area contain magnetite, in places at high concentrations, and the high-grade ore zone is characterized by a clear overprint of hematite replacing magnetite. Much of this magnetite formed early (during D_1 and D_3 stage 1 alteration; Tables 1 and 2) as the product of metamorphism and early metasomatism, and its presence clearly played a role in the precipitation of hematite, and by extension, possibly gold. Thus, early gold precipitation during D_1 may have involved a reaction between magnetite and the altering high temperature fluids, but direct textural evidence for this has not been found.

The most characteristic feature of the high-grade ore zones in all lithologies is the high degree of silicification, which occurred both early (D_1) with silicification concentrated along the hanging wall quartzite, and late (D_3) with the formation of a dense network of syn-D_3, laminar veins that are mostly thin (<0.5 cm) and both parallel and transect the underlying S_1 fabric. The fine, laminar D_3 veins have the appearance of quartz ribbon grains thereby masking the extent of their development in quartz-feldspar mylonite. Sodic, and potassic alteration with the development of albite and later K-feldspar-sericite was part of this process. In most places micro-fractures associated with the veining were healed, but their imprint remains visible as trails of fluid inclusions, alteration minerals, and gold grains.

Thus, the main lithological control on the configuration of the deposit with respect to the late gold stage and the lower temperature D_3 alteration events appears to have been mechanical in nature, in which strongly silicified lithologies were preferentially fractured. The competency of the lithologies resulted in part from the high-grade metamorphic nature (i.e. coarse-grained, granoblastic, mica-poor) of the rock in combination with the effects of at least two periods of pervasive silicification (early D_1 and early D_3) that affected the ore zone prior to D_3 fracturing and (re-)mobilization of the gold.

5.1.2. Structural controls

The geometry of the Tick Hill deposit is controlled by structures. $D_{1\text{-}2}$ shearing, folding and transposition led to the formation of tight intrafolial folds and foliation truncation planes, which occur as macro-scale shear bands; a phenomenon common in high-grade gneiss belts (e.g. Dirks and Wilson, 1995; Passchier and Trouw, 2005). It also included the formation of laterally continuous mylonitic quartz-rich zones interpreted as silicified and altered, syn-D_1 shear horizons (e.g. Laing, 1993; Tedman-Jones, 2001; Le, 2021) represented in Tick Hill by the hanging wall quartzite. These structures provided the architecture into which gold mineralization was introduced.

On the scale of the deposit (i.e. 100 m scale) the distribution of the ore zone coincides with a D_1 foliation truncation plane (Fig. 3a), and early gold was probably concentrated along this surface. The D_1 foliation truncation plane was reactivated during D_3, as part of a network of faults and veins that created the fluid pathways through which later hydrothermal fluids were channeled that had the capacity to remobilize early gold, or transport and introduce late gold.

Exploration reports for the deposit have suggested that the linear, east-northeast-plunging, high-grade ore zone parallels the dominant mineral elongation lineation (L_{1x}) and this has been used as an argument for early gold mineralization (e.g. Choy, 1994; Oliver, 1998). Our observations indicate that the linear high-grade ore envelope more-or less parallels the L_{1x} mineral lineation, but it also coincides with the orientation of the intersection lineation between two sets of D_3 faults and associated veins, i.e. a north-northeast-trending set, and an east-trending set (Fig. 6c). The main north-northeast-trending fault paralleled the D_1 foliation truncation plane and the mylonitic fabric west of the fault, and the high-grade ore envelope coincides with it. The east-trending fracture set provided a second order (10 m scale) control on D_3 fluid migration. The coincidence of low-grade (<0.1 g/t) ore envelopes with some of these east-trending fractures away from the main ore zone, indicate that at least some of the gold moved along these fractures during D_3; the question is “by how much ?”.

On the scale of individual outcrops, high-grade gold domains are dominated by numerous, laminar D_3 fractures that either parallel the main S_1 mylonitic fabric or occur as steep, east-trending partings to create the stock work vein pattern that is texturally associated with late gold. Gold occurs inside D_3 fractures and veins, and is commonly intergrown with D_3 alteration assemblages, linking the distribution of gold to D_3 structures on mm- to m-scales. However, coarse gold aligned in S_1 is commonly surrounded by a halo of fine gold, suggesting that early gold re-mobilized during D_3 and did not necessarily travel far to be re-deposited as late gold.

The textural observation that late gold may not have moved far, taken together with the spatial coincidence of the ore body with L_{1x} and the D_1 foliation truncation plane, and the sharp boundary of the high-grade ore shell, indicate that gold remobilization during D_3 may only have had a limited spatial effect. It suggests that the large-scale

distribution of gold at Tick Hill must be understood in terms of controlling $D_{1\text{-}2}$ structures.

5.2. The stress field during mineralization

The nature of the stress field at the time of mineralization may have provided a further control on gold deposition, at least during the D_3 stages of mineralization. Early models for the Tick Hill deposit have suggested that the mineralization formed during D_1 in an extensional environment (e.g. Laing, 1993; Choy, 1994). Later, Tedman-Jones (2001) suggested that gold was controlled by activity on the Plum Mt. and Mt. Bruce Faults (Fig. 2a), due to E-W compression during D_3 (Forrestal et al., 1998).

The strongly annealed and complex nature of $D_{1\text{-}2}$ structures and lack of kinematic indicators precludes reliable statements regarding the nature of the stress field during deposition of early gold. This is different for D_3 when late gold was mobilized. The shear indicators that exist along the main north-northeast-trending D_3 fault suggest a sinistral-normal sense of movement, whilst the east-trending D_3 faults that are well exposed in the northwest corner of the pit, preserve clear normal components of movement (Fig. 7e). Given that the mineralization of late gold can be linked to these faults, both within the pit and in drill core, D_3 alteration and late gold mobilisation probably occurred during extension. The cause of extension at Tick Hill during D_3 is unresolved. It could reflect a localized effect, e.g. extension above an intrusive body, or it could have resulted from a regional extensional event.

5.3. The potential role of intrusions

Exploration reports in the early 1990s have suggested that early gold mineralization was caused by the syn-D_1 emplacement of granites belonging to the Tick Hill intrusive suite (e.g. Tedman-Jones, 2001). This potentially included the quartz-feldspar mylonite that hosts much of the gold at Tick Hill. However, because of the high-grade metamorphic overprint during $D_{1\text{-}2}$ and the pervasive hydrothermal alteration during D_3, a genetic link between these strongly deformed and altered granites and early gold is hard to proof other than pointing at a spatial and temporal correlation.

Arguments for possible intrusive activity during the formation of late gold are stronger. The occurrence of pegmatite veins and quartz-feldspar metasomatism in the high-grade ore zones, as well as the apparent association of gold with Bi-Cu and oxidizing fluids, can be interpreted as indications of intrusion-related gold mineralization (e.g. Thompson et al., 1999; Hart and Goldfarb, 2005). Aeromagnetic data collected by MIM during the 1990s showed that the Tick Hill orebody is located at the northeast margin of a 3 × 2 km, oval shaped magnetic low that was interpreted as a possible concealed intrusion (Nano, 1999), potentially linking mineralizing fluids to a granite intrusion at depth (Tedman-Jones, 2001). Other than the late pegmatite bodies described here, no late-tectonic granite bodies were found in the area (Wyborn, 1997; Laing, 1993). The late pegmatite intrusions around Tick Hill are granitic in composition and were emplaced during D_3. The stage 2 (D_3) feldspar-rich sheeted veins are similar in composition and timing to the late pegmatite veins, and they are common in drill core below the ore zone. These sheeted veins occur with fracture zones, and in part involved a metasomatic overprint of the surrounding gneiss. They share the same deformation textures and are associated with similar alteration haloes as the late pegmatite bodies visible in the pit, and therefore, late pegmatite and late gold mineralization could be related to syn-D_3 igneous activity. Oxygen isotope data obtained from lithologies in and around the deposit, have been cited as evidence for an intrusive fluid (e.g. Choy, 1994). However, the $\delta^{18}O_{VSMOW}$ values vary little (+10.2 to +12.9‰, Hannan, 1994; Le, 2021) across a variety of rock types and veins, and they do not unequivocally reflect a magmatic source (e.g. Oliver et al., 2004).

A further argument that can be made for the possible involvement of an intrusive body at depth during late gold mineralization is the stockwork-like geometry of the fracture-networks and veins that host the gold at Tick Hill (Fig. 7c,e). Vein distribution patterns can reflect the broader geological setting during fluid migration; e.g. intrusion-related, low- and high-sulfidation gold deposits that formed from fluids released by a causative intrusion typically display widespread stockwork veining across all lithologies (e.g. Corbett and Leach, 1998; Thompson et al., 1999; Corbett, 2002; Rowe and Zhou, 2007; Goldfarb and Groves, 2015; Blenkinsop et al., 2020), rather than showing a systematic distribution of secondary structures near a master fault typical for orogenic gold deposits (e.g. Colvine et al., 1988; Goldfarb et al., 2005; Blenkinsop et al., 2020; Dirks et al., 2013, 2020). At Tick Hill, the mineralized D_3 veins, fracture networks and associated breccia zones are highly localized and stock-work like, whilst any through-going controlling D_3 shear zones are absent. Additionally, the five different stages of alteration and veining observed during D_3, suggest that brecciation and fracturing was a process that repeated itself several times, and involved a number of fluid pulses as the temperature of the altering fluid was cooling (Table 2). These observations are consistent with the presence of an igneous intrusion below Tick Hill, which could have driven episodic fluid flow through a network of D_3 structures and remobilized early gold, and/or introduced late gold.

5.4. Timing of mineralization

Although most of the mineralization at Tick Hill when viewed on mm- to m- scales is related to D_3 fracture zones and associated laminar veins and quartz-albite-hematite-chlorite alteration (Table 2), not all observations fit this pattern. In particular, the presence of coarse-grained, granoblastic gold inclusions in seemingly unaltered peak-metamorphic scapolite, hornblende and clinopyroxene grains that are aligned within S_1 contradicts D_3 gold mineralization. The presence of early gold in peak-metamorphic minerals was cited by Choy (1994), and has led to speculation during the early exploration stages that the mineralization must have predated the main $D_{1\text{-}2}$ events (Laing, 1993; Oliver, 1998; Tedman-Jones, 2001). In various exploration reports, it was suggested that the original source of mineralization could have been sedimentary-alluvial, syn-sedimentary epithermal, or associated with early stage intrusions that were subsequently sheared and mylonitised (Laing, 1993; England, 1993, 1995; Choy, 1994; Oliver, 1998). It is worth looking at each of these scenarios.

If a significant amount of the gold formed prior to or early during D_1, it is hard to explain the highly concentrated nature of the mineralization considering the intensity of the $S_{1\text{-}2}$ mylonitic transposition fabric and D_3 metasomatic overprint, unless the early gold forming event itself was highly localized. Regional exploration along strike, in litho-stratigraphic units that are similar to those hosting mineralization at Tick Hill, have not yielded any significant gold enrichment. This would make it unlikely that a significant amount of the gold at Tick Hill would have formed as alluvial gold in a sedimentary environment, or that it was associated with early intrusions, since both of these mechanisms would have likely resulted in a more dispersed distribution of early gold (e.g. Robb and Robb, 1998; Hart and Goldfarb, 2005; Tucker et al., 2016).

The most plausible explanation for the confined early deposition of gold, although based on limited evidence, has been the suggestion that gold was deposited from magmatic fluids in an extensional fault jog along D_1 shears that are represented by the quartzite ridges (e.g. Laing, 1993; Oliver, 1998; Tedman-Jones, 2001), with fluids moving along the L_{1x} mineral elongation direction. This would have happened at the same time that granite was emplaced, which is represented by the quartz-feldspar mylonite that hosts much of the mineralization. Mapping of the quartzite ridges in the Tick Hill area has demonstrated that many of them transgress the dominant gneissic layering, and are strongly metasomatized (e.g. magnetite rich) with lensoidal geometries, gradational margins and fringed terminations suggesting alteration fronts (Coughlin, 1993; Laing, 1993; Le, 2021). Few unequivocal sedimentary

structures have been described from any of the quartzite ridges in the region, and many are characterized by extensive micro-veining, brecciation and silicification, largely masked by later recrystallization and metasomatism. This is the case for the hanging wall quartzite at Tick Hill, which was, therefore, interpreted as a strongly silicified metasomatized D_1 shear zone (e.g. Coughlin, 1993; Laing, 1993; Le, 2021). Mapping presented here suggests that the D_1 foliation truncation plane that resembles an extensional shear band in the immediate footwall of the hanging wall quartzite, may have provided the dilatational site needed for gold deposition.

In spite of overwhelming structural evidence that the host rocks are mylonitic, the laminate textures in the Tick Hill ore zone have also been interpreted as primary varve-like deposits from silica gels in an epithermal environment (e.g. England, 1995). This interpretation followed suggestions of an epithermal exhalative origin for the gold-rich IOCG deposits at Starra (e.g. Davidson et al., 1989) ~60 km east of Tick Hill, but there is no evidence to support this.

Given the intensity of the later deformation and D_3 metasomatism, it is impossible to confidently pick the exact model that resulted in the deposition of early gold at Tick Hill. Structural arguments presented above suggest that the large-scale geometry of the ore zone is primarily controlled by D_1 structural elements, and that D_3, whilst pervasive at outcrop scales, only resulted in localized remobilization of early gold. These observations suggest that most if not all the gold at Tick Hill is early, even though the bulk of the mineralization when viewed in drill core, hand specimen or thin section is hosted by D_3 structures.

5.5. Constraints on the mineralizing fluids and mineralization style

One of the most characteristic alteration features associated with late gold mineralization at Tick Hill is the destruction of the magnetic signature in the lithologies that host the gold, as a result of the replacement of $D_{1\text{-}2}$ and stage 1 magnetite by hematite (Figs. 5c, 8). The abundance of hematite over magnetite in association with gold reflects the strongly oxidized nature of the D_3 hydrothermal fluids. In spite of this, the immediate hanging wall to the orebody is strongly enriched in magnetite, but most of this magnetite was texturally early, and probably associated with the formation of early gold, and it predated the pervasive late alteration and gold mineralization.

Similar to magnetite, sulfides appear to have been affected and largely resorbed in the high-grade ore zones, presumably by the same late stage (D_3) hydrothermal fluids. Gold observed in stage 2 to stage 4 assemblages, occurs everywhere as free gold, readily visible under the microscope, and generally associated with little or no sulfide. In some of the more mafic lithologies (e.g. amphibolite-bearing calc-silicate), gold occurs in spatial association with trace amounts of pyrite, chalcopyrite and pyrrhotite, but these sulfides are typically irregular, strongly embayed, and skeletal in shape, although in some places gold is intergrown with newly formed subhedral pyrite or pyrrhotite. Instead, gold is more commonly associated with Bi-selenides. These observations suggest that most sulfides represent the remains of older grains that may have formed with early gold and predated late gold mineralization when sulfide was largely resorbed and removed from the high-grade ore-zones by S-under-saturated fluids.

Pyrite, chalcopyrite and pyrrhotite patches are common in amphibolite and amphibolitic calc-silicate units in the hanging wall and footwall to the deposit. Although there is no obvious metal enrichment other than gold within the ore zone itself, a weak Co (>30 ppm) anomaly has been observed, whilst the immediate footwall to the high-grade mineralized zone, typically showed enrichment in Cu (>200 ppm). On a local scale, Cu and Co show a poor spatial correlation with gold in assay data, whilst Co and Cu correlate with each other and with Ni. The observed Cu-Co enrichment correlates with chalcopyrite-pyrite mineralization in the footwall. What is not clear is whether this chalcopyrite-pyrite mineralization formed with the late gold as part of the mineralizing fluids, or whether Cu and Co were present in the host rock prior to oxidizing fluids leaching the host rock of its metals during D_3. In other words, similar to magnetite being largely destroyed by the late stage oxidizing fluids, sulfides in the host rocks may have also been destroyed with S and Cu and to a lesser degree Co being removed from the high-grade gold zone as early gold was remobilized at a more localized scale. The Cu-sulfides were subsequently redeposited along the edges of the mineralization, presumably as a result of the interaction of the mineralizing fluids with the ambient fluids. This would be consistent with the sulfide textures and the gold-only nature of the ore. It is also consistent with early gold being re-mobilized by the same fluids to be redeposited as late gold along D_3 structures.

Apart from hematite, the gold-rich zone is characterized by quartz-albite-oligoclase-K-feldspar-sericite alteration, which showed a temporal evolution from early sodic alteration dominated by albite (stage 1 and early stage 2) to later, more potassic alteration with the formation of K-feldspar and sericite (late stage 2 and stage 3). The ore zone is further characterized by a recrystallized granoblastic texture in quartzo-feldspathic rocks. The bulk of the gold as preserved today was deposited during D_3 in stage 2, with stage 3 and 4 mineralization being either due to the continued inflow of new gold, or the remobilization of stage 2 gold (Table 2). However, as argued above, even stage 2 gold probably largely originated from the remobilization of early gold, and little, if any, gold may have been introduced during D_3.

The alteration mineral assemblage that formed during stage 1 (i.e. magnesio-hornblende, albite, oligoclase) indicates that D_3 metasomatic events started at upper-greenschist facies conditions. The assemblages that formed during stage 2 (actinolite, albite, $chlorite_1$), stage 3 ($chlorite_2$, epidote, K-feldspar, sericite) and stage 4 ($chlorite_3$, calcite) indicate a progressive drop in temperature of the hydrothermal fluids. The intense hematite alteration, the formation of leucoxene and selenides, and the destruction of magnetite (Fig. 8) and sulfide indicate that the mineralized fluids were strongly oxidized and S-under-saturated during stages 2 and 3. Conditions may have varied somewhat with the localized formation of pyrrhotite after pyrite suggesting more reduced conditions in at least parts of the deposit. This type of textural variation could reflect the interplay of reduced mineralizing fluid with a more oxidized ambient fluid considering the regional prevalence of hematite as an alteration phase (e.g. Oliver, 1995; Skirrow and Walshe, 2002). The fact that carbonates are largely absent from the alteration assemblage would further suggest that the fluids that mobilized gold during D_3 did not contain CO_2. These constraints on the fluid composition indicate that late gold was not transported as a bisulfide complex, but must instead have moved as halogen complexes at low pH conditions. This is likely to have involved chlorine as is common in IOCG deposits in the Mt Isa district (e.g. Williams et al., 2001, 2005; Williams and Pollard, 2001; Oliver et al., 2004) and considering the presence of Cl in stage 1 amphibole (Le, 2021). Thus, the late stage, low temperature mineralizing fluids that remobilized early gold during D_3 were saline and oxidized, a characteristic that has been linked to igneous activity (e.g. Oliver et al., 2004; Mark et al., 2006).

One conspicuous feature about the Tick Hill deposit is the presence of a range of selenide minerals and the corresponding general paucity of sulfides in direct association with gold. Selenide minerals are relatively rare in mineral deposits, because Se, which is strongly chalcophile, readily substitutes for sulfur in sulfide minerals. Deposition of selenides, rather than substitution in e.g. pyrite or chalcopyrite, therefore, requires specific conditions, and the selenide mineral assemblage places constraints on the nature the ore forming fluids as well as physical conditions of formation (e.g. Simon and Essene, 1996; Simon et al., 1997; Cook et al., 2009; Cabral et al., 2017). Bi-Cu-Pb bearing selenide deposits with hematite and rare sulfides have been described from vein deposits in schists, where they typically formed at relatively low temperatures from highly oxidized saline fluids within the hematite stability field at a low sulfur fugacity (e.g. Simon et al., 1997; Cabral et al., 2017). A high oxygen fugacity prevents the early incorporation of Se in sulfides and promotes the formation of selenides, which generally occurs

between 65 and 300 °C, and mostly below 150 °C (Simon et al., 1997). Reconstructions of the palaeo-depth of most selenide-bearing deposits indicate that lithostatic pressures were probably <0.5 kbar (Simon et al., 1997). The formation of selenides of elements such as Cu require acidic or reducing environments (Cook et al., 2009). Thus, the presence at Tick Hill of Bi-Cu-Pb selenides in association with gold probably indicates a relatively shallow formational depth at relatively low temperatures, and it further confirms the involvement of strongly oxidized, acidic, saline fluids in which gold and other metals (Bi, Cu, Ni, Co) were mobilized as chlorine complexes (Simon et al., 1997; Cook et al., 2009). Some of the selenides at Tick Hill contain minor Te as well, and the association Au-Bi-Te-Se, together with other chalcophile elements has been linked to a magmatic signature (e.g. Spooner, 1993).

5.6. An alternative model for gold at Tick Hill

The alteration assemblage and structural setting at Tick Hill display some similarities with IOCG deposits in the Eastern Fold Belt of the Mt Isa Inlier (e.g. Williams et al., 2005), but these mostly relate to D_3 alteration and the mobilization of late gold. Similarities include the strong structural controls on mineralization, the prevalence of sodic alteration predating late gold mineralization and the shift from sodic to more potassic alteration as gold deposition progresses, the presence of abundant hematite and magnetite together with chlorite in association with gold, and the involvement of oxidized, acidic saline fluids (e.g. Williams, 1998; Williams and Pollard, 2001; Oliver et al., 2004; Williams et al., 2005; Groves et al., 2010; Mclellan et al., 2010). But there are important differences with classic IOCG deposits in the eastern fold belt (e.g. Groves et al., 2010). These include the absence of any significant copper mineralization, or any other significant metal enrichment for that matter, the absence of significant sulfide mineralization, the presence of Bi-selenides, and the absence of large volumes of concomitant felsic or mafic intrusions in the area at least during D_3 (Oliver et al., 2004, 2008). The high-grade metamorphic nature of the host rock and the high gold-grade and extremely restricted nature of the deposit also differ from IOCG deposits in the Eastern Fold Belt. Thus, the geological setting of Tick Hill does not provide an easy match with any existing deposit type in the Mt Isa Inlier.

When considering the Au-rich nature of the Tick Hill deposit, its association with Bi and Se and extensive hematite-chlorite alteration, the Tick Hill deposit displays many similarities with some of the high-grade gold deposits (e.g. Nobles Nob; Eldorado; Skirrow and Walshe, 2002; Groves et al., 2010) in the Tennant Creek area of the Northern Territory, Australia. The Tennant Creek gold field includes a large range of Au-Cu-Bi deposits that vary significantly in Au:Cu ratios, Fe-oxide and sulfide mineralogy and isotope compositions, and include reduced Cu-rich, and oxidized Au-rich end-members (Skirrow and Walshe, 2002; Groves et al., 2010). The Cu-rich endmember deposits have been considered as possible IOCG deposits (e.g. Skirrow, 2000; Williams et al., 2005). In contrast, the Au-rich end-member deposits do not comfortably fit in the IOCG family (Groves et al., 2010), but they compare favorably with Tick Hill (e.g. Groves et al., 2010). Mineralization in the Tennant Creek area comprises native gold, chalcopyrite, and a range of bismuth minerals including S-Se-Te-Cu-Pb-bearing Bi sulfosalts (Large, 1975; Wedekind et al., 1989; Skirrow and Walshe, 2002). The Au-rich deposits (e.g. Juno, Argo, Nobles Nob, Eldorado deposits) tend to have minor to abundant hematite alteration of pre-existing magnetite and widespread chlorite, muscovite, pyrite alteration (Skirrow and Walshe, 2002). The mineralization is typically hosted by structurally controlled, magnetite/hematite-rich, hydrothermal replacement bodies referred to as 'ironstones' that formed at temperatures of 350–400 °C and 2.5–5.0 kbars (Skirrow and Walshe, 2002). These 'ironstones' are hosted by ca. 1860 Ma, low-grade metasedimentary turbidites. The Au-Cu-Bi mineralization was introduced into the ironstone bodies at slightly lower temperatures (~300 °C) during the regional Tennant Event at 1860–1845 Ma (Compston and McDougall, 1994; Skirrow and Walshe, 2002). The Au-rich deposits have been linked to reactions between magnetite ironstone and oxidizing brines that mixed with pulses of intermediate-oxygen fugacity, low- to moderate-salinity ore fluids to deposit gold and Bi sulfosalts whereas Cu deposition was suppressed by increasing solubility of Cu in the mixed fluid (Skirrow and Walshe, 2002). Additional significant 'non-ironstone' deposits of Au-Cu-Bi mineralization occur within shear zones outside the ironstones (e.g. Orlando East, Navigator 6; Skirrow, 2000; Skirrow et al., 2019). Some of the shear zone hosted deposits were dated at ca. 1660 Ma and are thought to have formed through remobilization of the main ironstone-hosted Au-Cu-Bi ore bodies with Au moving up to 100 s of meters (Skirrow et al., 2019). A ubiquitous feature of the gold-bearing veins is the presence of chlorite alteration adjacent to the veins together with hematite, monazite and chalcopyrite.

At Tick Hill it would appear that highly oxidized, Bi-Se-bearing hydrothermal fluids active during D_3, were capable of transporting late gold to its current depositional sites. The presence of gold in hornblende and clinopyroxene grains that are aligned in the D_1 fabric, indicates that this gold mineralization may originally have occurred early. If one considers the parallels that exist with the Tennant Creek gold field, we suggest that there is a genuine possibility that early high-grade Au-Cu-Bi mineralization of the oxidized Au-rich end-member type (Skirrow and Walshe, 2002) may have formed either before or during D_1. During $D_{1\text{-}2}$ this early gold mineralization was aligned with or formed in parallelism with D_1 structures and it overprinted syn-$D_{1\text{-}2}$ intrusions now preserved as quartz-feldspar mylonite. If this early gold mineralization was subsequently reworked and overprinted by low temperature hydrothermal fluids with the capacity to remobilize metals including gold, then the Tick Hill deposit could represent a remobilized, older high-grade gold deposit. The fluids involved in this remobilization were highly saline, oxidized fluids that gave rise to the extensive regional albite-hematite alteration in the area (e.g. Oliver, 1995). These fluids would not necessarily have to be gold-rich, but could have scavenged their metal load from the older deposits in a way described for the late Au-vein deposits in the Tennant Creek area (Skirrow et al., 2019).

6. Conclusions

Four deformational events have been recorded at Tick Hill and the surrounding rocks including: (1) regional D_1 shearing resulting in the formation of mylonitic textures at high-grade metamorphic conditions; (2) D_2 upright folding that formed the Tick Hill syncline, again at high-grade metamorphic conditions; (3) D_3 oblique-normal faulting with extensional veining and widespread quartz-feldspar alteration near Tick Hill and subsequent regional red rock alteration; and (4) D_4 strike-slip faulting with cataclasite textures. The ore zone at Tick Hill parallels a D_1 foliation truncation plane that was reactivated during D_3 sinistral-normal faulting. Mineralization also approximately parallels the L_{1x} mineral elongation lineation, and the intersection lineation between sets of D_3 faults, with localized brecciation along the faults increasing with depth.

Key features of gold mineralization at Tick Hill include: (1) the high-grade, coarse-grained, gold-only nature of the deposit most of which was deposited in its current textural position during D_3 faulting and associated alteration (late gold); (2) the presence of an early, pre- or syn-D_1 stage of mineralization (early gold); (3) the restricted nature of the deposit, with an abrupt boundary between mineralized and non-mineralized zones; (4) a paucity of sulfides and other metals in the ore zone together with the presence Bi-selenides in association with late gold; (5) a prevalence of magnetite and hematite, with hematite concentrated in the ore zone; (6) early (D_1) high-temperature alteration assemblages characterized by magnetite and quartz, possibly associated with early gold; (7) late (D_3) low-temperature alteration assemblages characterized by proximal amphibole, albite, hematite, chlorite, epidote, sericite, illite, and minor calcite, and associated with late gold; (8) proximal mineralization coincided with D_3 brecciation and intense

silicification, bounded by a strongly silicified zone and surrounded by a chlorite-epidote shell; (9) the presence of abundant laminar quartz veins, locally forming breccia associated with late gold; (10) the involvement of strongly oxidized, acidic, saline, hydrous fluid during late (D_3) low-temperature alteration; and (11) a possible genetic relationship between syn-D_3 pegmatite and late-stage alteration fluids.

In terms of alteration assemblages and structural setting the Tick Hill deposit shares many similarities with the ca.1850 Ma, Au-Cu-Bi mineralization in the Tennant Creek area. Its high-grade gold-only nature, lack of significant Cu enrichment, presence of Bi-selenides and general absence of associated intrusions make it a unique deposit in the Mt Isa Inlier. Evidence of early mineralization and D_3 related remobilization of gold and sulfides suggest that early gold enrichment was responsible for the bulk of the mineralization and it was remobilized by later hydrothermal fluids to be deposited as late gold in suitable structural traps during D_3.

Declaration of Competing Interest

The authors declare that they have no known competing financial interests or personal relationships that could have appeared to influence the work reported in this paper.

Acknowledgements

We would like to thank the Geological Survey of Queensland and the Economic Geology Research Centre (EGRU, James Cook University) who provided support to conduct this study. We would like to thank Peter Rea, Alex Brown from Glencore, Mount Isa Mines and Paul Tan, Brett Davis and Rob Watkins from Carnaby Resources for providing logistical support for fieldwork, access to drill core and data sets. Our thanks to Nick Oliver for donating Tick Hill samples for this study. Nick Oliver and a second reviewer are also thanked for their critical and constructive reviews, which helped improve the manuscript. We acknowledge the assistance of the Advanced Analytical Centre (James Cook University) for geochemical analyses. Our thanks to Kaylene Camuti for help with editing early versions of the manuscript. Funding for this study was provided by the Department of Natural Resources, Mines and Energy.

Appendix A. Supplementary data

Supplementary data to this article can be found online at https://doi.org/10.1016/j.oregeorev.2021.104288.

References

Aeon Metals Limited, 2017. Zambian Copperbelt-style geological model - a revised Walford Creek geological model. Exploration Report. <https://www.aeonmetals.com.au/assets/uploads/2017/07/2017-Jul-28-Zambian-Copperbelt-Style-Geological-Model.pdf>.

Babo, J., Spandler, C., Oliver, N.H.S., Brown, M., Rubenach, M.J., Creaser, R.A., 2017. The high-grade Mo-Re Merlin deposit, Cloncurry district, Australia: Paragenesis and geochronology of hydrothermal alteration and ore formation. Econ. Geol. 112 (2), 397–422.

Betts, P.G., Giles, D., Mark, G., Lister, G.S., Goleby, B.R., Aillères, L., 2006. Synthesis of the Proterozoic evolution of the Mt Isa Inlier. Aust. J. Earth Sci. 53 (1), 187–211.

Blake, D.H., Bultitude, R.J., Donchak, P.J.T., 1982. Dajarra, Queensland 1:100000 geological map commentary. BMR Geol. Geophys. 225, 83 pp.

Blake, D.H., 1987. Geology of the Mount Isa inlier and environs, Queensland and Northern Territory. BMR Geol. Geophys. Aust. Bull. 225, 1–83.

Blake, D., Steward, A., 1992. Stratigraphic and tectonic framework, Mount Isa. AGSO Bull. 243, 1–11.

Blenkinsop, O., Dirks, P.H.G.M., Nugus, S.I.V., Tripp, G., 2020. Structural Geology applied to the evaluation of Hydrothermal Gold Deposits. SEG Rev. Econ. Geol. 21, 1–23.

Cabral, A.R., Ließmann, W., Jian, W., Lehmann, B., 2017. Selenides from St. Andreasberg, Germany: an oxidised five–element style of mineralization and its relation to post–Variscan vein–type deposits of central Europe. Int. J. Earth Sci. (Geol Rundsch) 106, 2359–2369.

Carnaby Resources, 2021. Mount Isa Inlier Gold and Copper Projects. <https://carnabyresources.com.au/projects/mount-isa-inlier-gold-and-copper-projects/>.

Carson, C., Hutton, L., Withnall, I., Perkins, W., Donchak, P., Parsons, A., Blake, P., Sweet, I., Neumann, N., Lambeck, A., 2011. Summary of results: Joint GSQ-GA geochronology project, Mount Isa region, 2009–2010. Queensland Geological Record 2011/03.

Choy, D.K.W., 1994. The geology, structure, petrology, alteration and mineralization of Tick Hill, North-West Queensland. Master Thesis. Monash University, p. 220 pp..

Colvine, A., Fyon, J., Heather, K., Marmont, S., Smith, P., Troop, D., 1988. Archean lode gold deposits in Ontario. In: Ontario Geological Survey, Miscellaneous Paper, p. 136 pp.

Compston, D.M., McDougall, I., 1994. 40Ar/39Ar and K-Ar age constraints on the Early Proterozoic Tennant Creek Block, northern Australia, and the age of its gold deposits. Aust. J. Earth Sci. 41, 609–616.

Cook, N.J., Ciobanu, C.L., Spry, P.G., Voudouris, P., 2009. Understanding gold-(silver)-telluride-(selenide) mineral deposits. Episodes 32 (4), 249–263.

Corbett, G.J., Leach, T.M., 1998. Southwest Pacific Rim gold-copper systems: structure, alteration, and mineralization. In: Society of Economic Geologists, Special publication, p. 237 pp.

Corbett, G., 2002. Epithermal gold for explorationists. AIG News, 67, pp. 1–8.

Coughlin, T.J., 1993. Burke River; QLD; EPM 9083; Tick Hill Enclave 1:10000 Geological Mapping Programme. Internal MIMEX Report, Record No. 8548, Mt Isa exploration office.

Davidson, G., Large, R., Kary, G., Osborne, R., 1989. The BIF-hosted Starra and Trough Tank Au-Cu mineralization: a new stratiform association from the Proterozoic eastern succession of Mt. Isa, Australia. Econ. Geol. Monogr. 6, 135–150.

Day, R., Whitaker, W., Murray, C., Wilson, I., Grimes, K., 1983. Queensland Geology: A companion volume to the 1: 2,500,000 scale geological map (1975). Publications of the Geological Survey of Queensland, 383.

Denaro, T.J., Randall, R.E., Smith, R.J., 2013. Chapter 10: mineral and energy resources. In: Jell, P.A. (Ed.), Geology of Queensland, Geological Survey of Queensland, Brisbane, pp. 687–762.

De Jong, G.D., Williams, P.J., 1995. Giant metasomatic system formed during exhumation of mid-crustal Proterozoic rocks in the vicinity of the Cloncurry Fault, northwest Queensland. Aust. J. Earth Sci. 42 (3), 281–290.

Dirks, P.H.G.M., Wilson, C.J.L., 1995. Crustal evolution of the East Antarctic mobile belt in Prydz Bay: continental collision at 500 Ma? Precambr. Res. 75 (3-4), 189–207.

Dirks, P.H.G.M., Charlesworth, E.G., Munyai, M.R., Wormald, R., 2013. Stress analysis, post-orogenic extension and 3.01Ga gold mineralization in the Barberton Greenstone Belt, South Africa. Precambrian Res. 226, 157–184. https://doi.org/10.1016/j.precam res.2012.12.007.

Dirks, P., Sanislav, I., van Ryt, M., Huizenga, J., Blenkinsop, T., Kolling, L., Kwelwa, S., Mwazembe, G., 2020. The world class gold deposits in the Geita Greenstone Belt, northwestern Tanzania. In: Sillitoe, R.H., Goldfarb, R.J., Robert, F., Simmons, S.F. (Eds.), Geology of the World's Major Gold Deposits Society of Economic Geologists, Special Publication, pp. 163–183.

Downs, R.C., 2000. Notes concerning thickness distributions of upper and lower quartzite horizons at Tick Hill and their control on gold mineralization. A down-plunge drill target. Internal report to MIM Exploration Pty Ltd, (B)CD.060, Record No. 20322, Mt Isa exploration office.

Duncan, R.J., Stein, H.J., Evans, K.A., Hitzman, M.W., Nelson, E.P., Kirwin, D.J., 2011. A new geochronological framework for mineralization and alteration in the selwyn-mount dore corridor, eastern fold belt, mount Isa Inlier, Australia: genetic implications for iron oxide copper-gold deposits. Econ. Geol. 106 (2), 169–192.

Duncan, R.J., Hitzman, M.W., Nelson, E.P., Togtokhbayar, O., 2014. Structural and lithological controls on iron oxide copper-gold deposits of the Southern Selwyn-Mount Dore Corridor, Eastern Fold Belt, Queensland, Australia. Econ. Geol. 109 (2), 419–456.

England, R.N., 1993. Petrographic report for 35 samples from Tick Hill. Report to MIM Exploration Pty Ltd. ISAMISREP.018, Record No. 30874, Mt Isa exploration office.

England, R.N., 1995. The Tick Hill sedimentary exhalative gold deposit. Report to MIM Exploration Pty Ltd. ISAMISREP.023, Record No. 30881, Mt Isa exploration office.

Etheridge, M., Rutland, R., Wyborn, L., 1987. Orogenesis and tectonic process in the Early to Middle Proterozoic of northern Australia. Proterozic Lithospheric Evol. 17, 131–147.

Forrestal, P., Pearson, P., Coughlin, T., Schubert, C., 1998. Tick hill gold deposit. Geology of the mineral deposits of Australia and Papua New Guinea. Australian Institute of Mining and Metallurgy, Carlton South, VIC, Monograph 22, pp. 699-706.

Foster, D., Austin, J., 2008. The 1800–1610Ma stratigraphic and magmatic history of the Eastern Succession, Mount Isa Inlier, and correlations with adjacent Paleoproterozoic terranes. Precambr. Res. 163 (1-2), 7–30.

Goldfarb, R.J., Baker, T., Dube, B., Groves, D.I., Hart, C.J., Gosselin, P., 2005. Distribution, character, and genesis of gold deposits in metamorphic terranes. In: Econ. Geol., 100th Anniversary, pp. 407–450.

Goldfarb, R.J., Groves, D.I., 2015. Orogenic gold: Common or evolving fluid and metal sources through time. Lithos 233, 2–26.

Groves, D.I., Bierlein, F.P., Meinert, L.D., Hitzman, M.W., 2010. Iron oxide copper-gold (IOCG) deposits through Earth history: implications for origin, lithospheric setting, and distinction from other epigenetic iron oxide deposits. Econ. Geol. 105 (3), 641–654.

Geological Survey of Queensland, 2015. Hyperspectral data for drill hole TH007RD (71815), Tick Hill Deposit. Geological Survey of Queensland. <https://minesonlinemaps.business.qld.gov.au/SilverlightViewer/Viewer.html?Viewer=momapspublic>.

Hannan, K., 1994. Tick Hill District quartz oxygen isotope results. Report to MIM Exploration Pty Ltd, Memo.1996/024, Record No. 18742, Mt Isa exploration office.

Hart, C.J.R., Goldfarb, R.J., 2005. Distinguishing intrusion-related from orogenic gold systems. In: New Zealand Minerals Conference Proceedings, pp. 125–133.

Holcombe, R., Pearson, P., Oliver, N., 1991. Geometry of a middle Proterozoic extensional decollement in northeastern Australia. Tectonophysics 191 (3–4), 255–274.
Huston, D.L., Stevens, B., Southgate, P.N., Muhling, P., Wyborn, L., 2006. Australian Zn-Pb-Ag ore-forming systems: a review and analysis. Econ. Geol. 101 (6), 1117–1157.
Johnson, D., 2002. Tick Hill Abrief Review. Report to MIM Exploration Pty Ltd, ISAMISREP.208a, Record No. 31073, Mt Isa exploration office.
Kositcin, N., Bultitude, R.J., Purdy, D.J., 2019. Queensland Geological Record 2019/02. Summary of results. Joint GSQ-GA Geochronology Project: Mary Kathleen Domain, Mount Isa Inlier, 2018-2019. Queensland Geological Record 2019/02.
Mark, G., Oliver, N.H.S., Williams, P.J., 2006. Mineralogical and chemical evolution of the Ernest Henry Fe oxide–Cu–Au ore system, Cloncurry district, northwest Queensland, Australia. Miner. Deposita 40 (8), 769–801.
McLellan, J.G., Mustard, R., Blenkinsop, T., Oliver, N.H., McKeagney, C., 2010. In: Critical Ingredients of IOCG Mineralization in the Eastern Fold Belt of the Mount Isa Inlier: Insights from Combining Spatial Analysis with Mechanical Numerical Modelling. PGC Publishing, pp. 233–255.
Laing, W.P., 1992. The metasomatic development of the quartz-feldspar laminate gold hostrock at Tick Hill, Illustrated. Report to MIM Exploration Pty Ltd., ISAMISREP.010; Record No. 30862, Mt Isa exploration office.
Laing, W.P., 1993. Geology of the Tick Hill region, Mount Isa, with implications for exploration. Report to MIM Exploration Pty Ltd., ISAMISREP.017; Record No. 30870, Mt Isa exploration office.
Large, R.R., 1975. Zonation of hydrothermal minerals at the Juno mine, Tennant Creek goldfield, central Australia. Econ. Geol. 70 (8), 1387–1413.
Le, T.X., 2021. Geological characteristics, genesis and ore controlling factors of the Tick Hill Au deposit, Dajarra District, NW Queensland, Australia. PhD thesis. James Cook University, p. 187 pp..
Le, T.X., Dirks, P.H.G.M., Sanislav I.V., Huizenga, J.M., Cocker, H., Manestar, G.N., 2021. Geochronological constraints on the geological history and gold mineralization in the Tick Hill region, Mt Isa Inlier. Precambrian Res. Under review.
MacCready, T., Goleby, B., Goncharov, A., Drummond, B., Lister, G., 1998. A framework of overprinting orogens based on interpretation of the Mount Isa deep seismic transect. Econ. Geol. 93 (8), 1422–1434.
MIM, 1993. Geological maps of underground mine levels at Tick Hill Mine. Mount Isa Mines, Data Repository. Mt Isa exploration office.
MIM, 2000. Assay Data for Exploration Drill Holes from Tick Hill. Mount Isa Mines, Data Repository. Mt Isa exploration office.
Nano, S., 1999. Tick Hill geophysics, geology. Report to MIM Exploration Pty Ltd, Unnamed record, Mt Isa exploration office.
Nano, S., Croxford, B., Moloney, M., 2000. Poster of Tick Hill Petrology. Report to MIM Exploration Pty Ltd, Unnamed record, Mt Isa exploration office.
Neumann, N.L., Gibson, G.M., Southgate, P.N., 2009. New SHRIMP age constraints on the timing and duration of magmatism and sedimentation in the Mary Kathleen Fold Belt, Mt Isa Inlier, Australia. Aust. J. Earth Sci. 56 (7), 965–983.
O'Dea, M.G., Lister, G.S., Maccready, T., Betts, P.G., Oliver, N.H.S., Pound, K.S., Huang, W., Valenta, R.K., Oliver, N.H.S., Valenta, R.K., 1997. Geodynamic evolution of the Proterozoic Mount Isa terrain. Geol. Soc., London, Spec. Publ. 121 (1), 99–122.
Oliver, N.H., Rawling, T.J., Cartwright, I., Pearson, P.J., 1994. High-temperature fluid-rock interaction and scapolitization in an extension-related hydrothermal system, Mary Kathleen, Australia. J. Petrol. 35 (6), 1455–1491.
Oliver, N.H.S., 1995. Hydrothermal history of the Mary Kathleen Fold Belt, Mt Isa Block, Queensland. Austr. J. Earth Sci. 42 (3), 267–279.
Oliver, N., 1998. Tick Hill - Altered and deformed granites and Corella metasediments. Report to MIM Exploration Pty Ltd (Email form), Unnamed record, Mt Isa exploration office.
Oliver, N.H.S., Pearson, P.J., Holcombe, R.J., Ord, A., 1999. Mary Kathleen metamorphic-hydrothermal uranium-rare-earth element deposit: Ore genesis and numerical model of coupled deformation and fluid flow. Aust. J. Earth Sci. 46 (3), 467–484.
Oliver, N.H.S., Cleverley, J.S., Mark, G., Pollard, P.J., Fu, B., Marshall, L.J., Rubenach, M. J., Williams, P.J., Baker, T., 2004. Modeling the role of sodic alteration in the genesis of Iron Oxide-Copper-Gold Deposits, Eastern Mount Isa Block, Australia. Econ. Geol. 99 (6), 1145–1176.
Oliver, N., Butera, K., Rubenach, M., Marshall, L., Cleverley, J., Mark, G., Tullemans, F., Esser, D., 2008. The protracted hydrothermal evolution of the Mount Isa Eastern Succession: a review and tectonic implications. Precambr. Res. 163 (1-2), 108–130.
Page, R.W., 1978. Response of U-Pb Zircon and Rb-Sr total-rock and mineral systems to low-grade regional metamorphism in proterozoic igneous rocks, mount Isa, Australia. J. Geol. Soc. Aust. 25 (3-4), 141–164.
Page, R., 1983. Chronology of magmatism, skarn formation, and uranium mineralization, Mary Kathleen, Queensland, Australia. Econ. Geol. 78 (5), 838–853.
Passchier, C., 1986. Proterozoic deformation in the Duchess belt, Australia: a contribution to the BMR Mount Isa regional tectonic history program. Geol. Mijnbouw 65, 47–56.
Passchier, C.W., Williams, P.R., 1989. Proterozoic extensional deformation in the Mount Isa inlier, Queensland, Australia. Geol. Mag. 126 (1), 43–53.
Passchier, C., 1992. Geology of the Myubee area, Mt Isa Inlier, Queensland. Detailed studies of Mount Isa Inlier, pp. 199-208.
Passchier, C.W., Trouw, R.A., 2005. In: Microtectonics. Springer Science & Business Media, p. 366.
Pence, J.S., Sanislav, I.V., Dirks, P.H.G.M., 2020. 1750–1710 Ma deformation along the eastern margin of the North Australia Craton. Precambr. Res. 353, 106019.
Robb, L.J., Robb, V.M., 1998. Gold in the witwatersrand basin. In: Wilson, M.G.C., Anheausser, C.R. (Eds.), The Mineral Resources of South Africa. Handbook, Council for Geoscience, pp. 294–349.
Rowe, R., Zhou, X., 2007. Models and exploration methods for major gold deposit types. Proc. Explor. 7, 691–711.
Rutherford, N.F., 1999. First annual joint venture report to 1st January 2000 for exploration permits for minerals 9083, 11012 & 11013, Burke River Region, Mt Isa-Cloncurry District, North West Queensland, Technical Report No: 1. <https://geoscience.data.qld.gov.au/report/cr030650>.
Rutherford, N.F., 2000. Second annual joint venture report to 1st January 2000 for exploration permits for minerals 9083, 11012 & 11013, Burke River Region, Mt Isa-Cloncurry District, North West Queensland, Technical Report No: 2. <https://geoscience.data.qld.gov.au/report/cr031587>.
Simon, G., Essene, E.J., 1996. Phase relations among selenides, sulfides, tellurides, and oxides; I, Thermodynamic properties and calculated equilibria. Econ. Geol. 91 (7), 1183–1208.
Simon, G., Kesler, S.E., Essene, E.J., 1997. Phase relations among selenides, sulfides, tellurides, and oxides.II. Applications to selenide-bearing ore deposits. Econ. Geol. 92, 468–484.
Skirrow, R.G., 2000. Gold-Copper-Bismuth Deposits of the Tennant Creek District, Australia: A Reappraisal of Diverse High Grade Systems. In: Porter, T.M. (Ed.), Hydrothermal Iron Oxide Copper-Gold & Related Deposits: A Global Perspective. Austral. Min. Found, Adelaide, pp. 149–160.
Skirrow, R.G., Walshe, J.L., 2002. Reduced and oxidized Au-Cu-Bi iron oxide deposits of the Tennant Creek inlier, Australia: an integrated geologic and chemical model. Econ. Geol. 97 (6), 1167–1202.
Skirrow, R.G., Cross, A.J., Lecomte, A., Mercadier, J., 2019. A shear-hosted Au-Cu-Bi metallogenic event at ca. 1660 Ma in the Tennant Creek goldfield (northern Australia) defined by in-situ monazite U-Pb-Th dating. Precambr. Res. 332, 105402 https://doi.org/10.1016/j.precamres.2019.105402.
Spooner, E.T.C., 1993. Magmatic sulphide-volatile interaction as a mechanism for producing chalcophile element enriched, Archean Au-quartz, epithermal Au-Ag and Au skarn hydrothermal ore fluids. Geol. Rev. 7, 359–379.
Tedman-Jones, C.J., 1993. Gold dispersion and geochemistry at the Tick Hill gold deposit and implications for exploration, Mt Isa Inlier. Master of Science. James Cook University, NW Queensland, p. 122.
Tedman-Jones, C., 2001. Tick Hill core relogging review. Internal report to MIM Exploration Pty Ltd. Misc.2001/010, Record No. 30764, Mt Isa exploration office.
Thompson, J.F.H., Sillitoe, R.H., Baker, T., Lang, J.R., Mortensen, J.K., 1999. Intrusion-related gold deposits associated with tungsten-tin provinces. Miner. Deposita 34 (4), 323–334.
Tucker, R.F., Viljoen, R.P., Viljoen, M.J., 2016. A review of the Witwatersrand Basin - the world's greatest goldfield. Episodes 39 (2), 105–133.
Walters, S., Bailey, A., 1998. Geology and mineralization of the Cannington Ag-Pb-Zn deposit; an example of Broken Hill-type mineralization in the eastern succession, Mount Isa Inlier, Australia. Econ. Geol. 93 (8), 1307–1329.
Watkins, R., 1993. Deformation, felsic magmatism and alteration associated with the Tick Hill Gold Deposit, NW Queensland. B.Sc. Hons. Thesis. Monash University.
Wedekind, M.R., Large, R.R., Williams, B.T., 1989. Controls on high-grade gold mineralization at Tennant Creek, Northern Territory, Australia. Econ. Geol. Monogr. 6, 168–179.
Williams, P.J., 1998. Metalliferous economic geology of the Mt Isa eastern succession, Queensland. Aust. J. Earth Sci. 45 (3), 329–341.
Williams, P.J., Pollard, P.J., 2001. Australian Proterozoic iron oxide-Cu-Au deposits: An overview with new metallogenic and exploration data from the Cloncurry district, northwest Queensland. Explor. Min. Geol. 10 (3), 191–213.
Williams, P.J., Dong, G., Ryan, C.G., Pollard, P.J., Rotherham, J.F., Mernagh, T.P., Chapman, L.H., 2001. Geochemistry of hypersaline fluid inclusions from the Starra (Fe oxide)-Au-Cu deposit, Cloncurry District, Queensland. Econ. Geol. 96 (4), 875–883.
Williams, P.J., Barton, M.D., Johnson, D.A., Fontboté, L., De Haller, A., Mark, G., Oliver, N.H., Marschik, R., 2005. Iron oxide copper-gold deposits: Geology, space-time distribution, and possible modes of origin. Econ. Geol. 371–405.
Withnall, I., Hutton, L., 2013. Chapter 2: North Australian Craton, In: Jell, P.A. (Ed.), Geology of Queensland. Geology of Queensland, Geological Survey of Queensland, Brisbane, pp. 23-112.
Wyborn, L.A.I., 1997. Dajarra 1:100,000 digital geology, part of Mt Isa geological digital dataset. Updated by Geological Survey of Queensland 2011, 2015 and 2018. <http://pid.geoscience.gov.au/dataset/ga/30923>.
Wyborn, L., Page, R., Mcculloch, M., 1988. Petrology, geochronology and isotope geochemistry of the post-1820 Ma granites of the Mount Isa Inlier: mechanisms for the generation of Proterozoic anorogenic granites. Precambr. Res. 40-41, 509–541.
Xu, G., 1996. Structural geology of the Dugald River Zn-Pb-Ag deposit, Mount Isa Inlier, Australia. Ore Geol. Rev. 11 (6), 339–361.